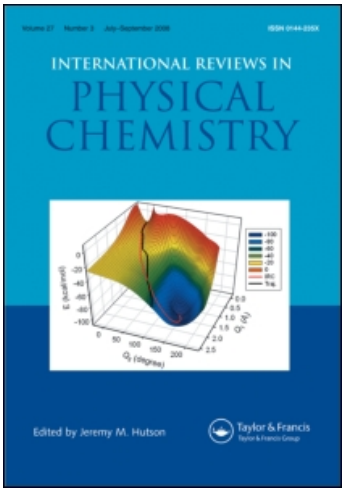

International Reviews in Physical Chemistry
Publication details, including instructions for authors and subscription information:
http://www.informaworld.com/smpp/title~content=t713724383

Optical properties and applications of dendrimer-metal nanocomposites

T. Goodson[a]; O. Varnavski[a]; Y. Wang[a]
[a] Department of Chemistry, Wayne State University, Detroit, MI 48202, USA

To cite this Article Goodson, T. , Varnavski, O. and Wang, Y.(2004) 'Optical properties and applications of dendrimer-metal nanocomposites', International Reviews in Physical Chemistry, 23: 1, 109 — 150
To link to this Article: DOI: 10.1080/01442350310001628875
URL: http://dx.doi.org/10.1080/01442350310001628875

INT. REVIEWS IN PHYSICAL CHEMISTRY, 2004
VOL. 23, NO. 1, 109–150

Taylor & Francis
Taylor & Francis Group

Optical properties and applications of dendrimer–metal nanocomposites

T. GOODSON III*, O. VARNAVSKI and Y. WANG
Department of Chemistry, Wayne State University,
Detroit, MI 48202, USA

The use of novel nanostructured materials for optical applications continues to be an important issue for the creation of new devices. New materials including metal nanoparticles have played an important role for applications in photonics, biology, as well as medicine. This review primarily concerns the use of one particular metal nanoparticle topology, dendrimer–metal nanocomposites. The focus of this review is to describe the optical properties of dendrimer–metal nanocomposites as well as functionalized dendrimer–metal nanocomposites. The description of various synthetic methodologies to produce transition metal (Au, Ag, Pd, Pt, and Cu) dendrimer nanocomposites as well as lanthanide ion-cored dendrimers are presented in this review, with further details regarding the basic characterization of these systems. The experimental procedures of the optical measurements used to probe the steady-state and time-resolved dynamics in these novel nanoparticle architectures are provided. Analysis of optical properties of dendrimer nanocomposites (DNCs) includes a description of the characterization of the metal nanoparticles as well as the size and distribution of metal nanoparticles formed by use of organic dendrimer template synthetic procedures (such as PAMAM). The non-linear transmission properties of certain dendrimer–metal nanocomposites show promising behaviour, which may be useful for applications involving eye and sensor protection. Reports of non-linear transmission properties of both Au and Ag dendrimer nanocomposites are discussed. Metal nanoparticles have also been suggested as useful materials for biological fluorescence imaging and sensing applications. However, it is well known that the efficiency of metal emission is very small. Recent measurements using ultra-fast spectroscopic techniques (fluorescence upconversion) have shed new light on this matter in metal nanoparticles and in dendrimer–metal nanocomposites. Dendrimer–metal nanocomposites have been used to investigate the dynamics of both metal particle emission and the interaction of metal particles with dipolar chromophores. The measurement and mechanism of ultra-fast transient absorption and emission dynamics in metal topologies including dendrimer nanocomposites are also discussed in the review. Future directions regarding the optical properties of dendrimer nanocomposites in the areas of photonics, biology, and medicine are also discussed in this review.

Contents

*Author to whom correspondence should be addressed. E-mail: tgoodson@chem.wayne.edu

International Reviews in Physical Chemistry ISSN 0144–235X print/ISSN 1366–591X online © 2004 Taylor & Francis Ltd
http://www.tandf.co.uk/journals
DOI: 10.1080/01442350310001628875

1. Introduction

1.1. *Background on optical effects in metal particles*

The search for new optical materials for device applications has inspired recent developments in the creation of nanostructured molecular architectures [1–4]. Optical applications involving light emission [5], non-linear optical effects [6], optical limiting [7], fluorescence imaging [8], and multi-photon absorption patterning [9] are just some of the examples that have already received technological attention. The types of materials used for these purposes range from organic polymers [10] and dendrimers [11], molecular crystals [12], as well as nanoparticle architectures [13]. While there has been a great amount of activity in regards to the details of the optical and electronic properties of semi-conducting nanoparticle architectures [14], there has also been recent attention to transition metal nanoparticle architectures [15]. The recent emphasis on nanotechnology has produced for investigation a number of new nanostructured metal topologies, which are created by a variety of successful procedures [16]. While the applications are indeed inspiring, it is important to note that the creation of metal particles with definite geometries and sizes (diameter) has also allowed for the systematic investigation of the fundamental optical excitations in metal objects [17–20]. Thus, the applications as well as the fundamental physics involved in the optical properties of metal nanoparticles have attracted a wide degree of interest [21]. Many of the optical applications of metal nanoparticles require a detailed understanding of their excited state and emission dynamics. In terms of the details of the optical excitations of metal nanostructures with different geometries, there have been many important investigations that have provided significant insight [22, 23]. Understanding the details of such processes is not only of fundamental interest but may also provide information regarding applications in surface enhanced Raman scattering [24], non-linear optics [25], as well as surface enhanced fluorescence [26].

1.2. *Common aspects of the preparation of metal nanostructures*

The preparation of metal nanoparticle systems has already established new directions for both science and technology. The synthesis and characterization of nanometre size metal nanoparticles have attracted substantial attention due to their optical, electrical and catalytic properties [27]. While gold particles of nanometer size have been synthesized since Faraday used surface-active molecules as stabilizers [28], templating approaches have come into focus over the last few years [29]. In these, polymers or pre-formed surfactant assemblies control size and shape of inorganic nanostructures. A well-established methodology used for the formation of metal nanoparticles is to use micelles of molecules, either surfactants or amphiphilic block copolymers where precursors are solubilized inside a self-assembled template [30, 31]. It has been reported by Antonietti and Gröhn that the templating of metal nanostructures can also be performed via an electrostatic approach in a hydrophilic aqueous solution using polyelectrolytes, e.g. polyelectrolyte microgels as templates [32]. In a precursor state, the polyelectrolyte microgel attracts oppositely charged metal ions which can be chemically reduced in a second step resulting in metal

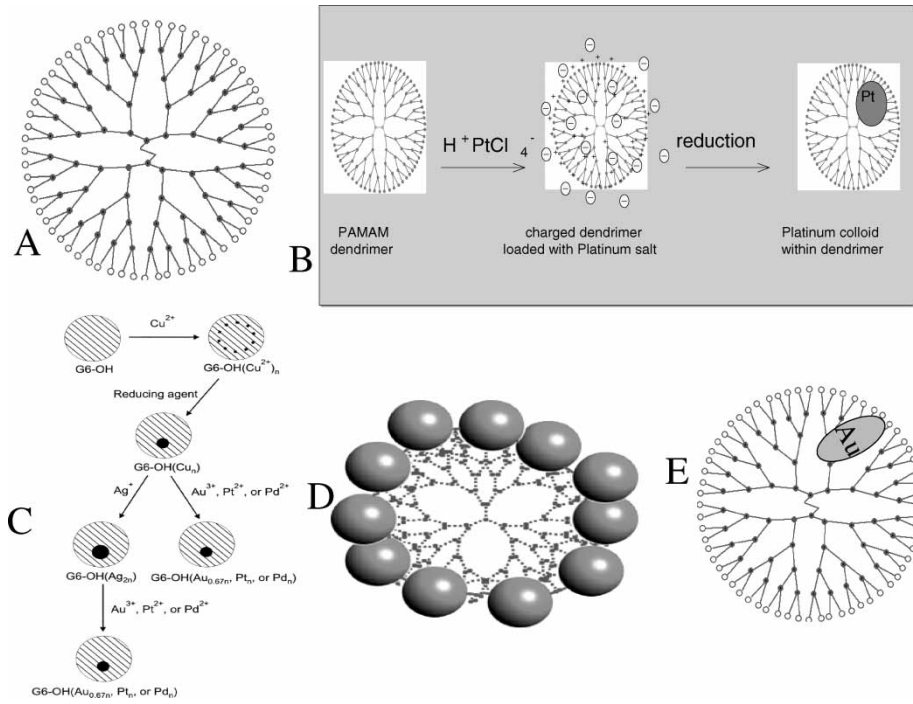

Figure 1. A: Structure of the host PAMAM dendrimer. B: Fabrication procedure for metal–dendrimer nanocomposites. C: Dendrimer encapsulated Au, Pd and Pt nanocomposites prepared by displacement reactions [104]. D, E: External and internal dendrimer nanocomposite topologies, respectively. Reprinted with permission from [104], copyright (1999) of the American Chemical Society, and from [113], copyright (1999) of Kluwer Academic Publishers B.V.

nanostructures embedded in the polyelectrolyte. Crooks, Balogh and Esumi have recently shown that polyelectrolyte dendrimers can be used as organic stabilizers or templates to produce a new type of nanocomposites [33–35]. It has been demonstrated that polyamine dendrimers can serve to form different metal colloids (zero-valent transition metals) and result in a variety of organic–inorganic hybrid architectures [36–41]. A schematic diagram of the PAMAM dendrimer host plus the formation and types of dendrimer–metal nanocomposites are shown in figure 1. The reported encapsulation can be accomplished in either an internal (figure 1E) or external (figure 1D) configuration. Furthermore, these dendrimer–inorganic nanocomposites incorporating transition metal particles have already shown to be of interest for a variety of applications, in particular as selective catalysts for both hydrogenation of alkenes in methanol/water solution and electrocatalysts for O_2 reduction [42, 43], as well as markers in biologic [44] and polymeric systems [45, 46]. Furthermore, these novel structures have shown impressive optical-limiting behaviour [47] as well as enhanced emission [48].

1.3. *Investigations of novel lanthanide ion-cored dendrimers*

Transition metals are not the only metals employed in dendrimer nanocomposites. Rare earth metals have also been considered in connection with emission in dendrimers, and in most cases lanthanide ions have been used for this purpose [49].

The chelation of a luminescent lanthanide ion into the core of a dendrimer can lead to new molecular architectures, capable of demonstrating novel and unusual optical properties [50]. In particular, the organic lanthanide systems demonstrate promising applications in optical fibre lasers and amplifiers [51], electroluminescent materials [52], and sensors [53]. The ability to efficiently encapsulate lanthanide metal ions into dendrimers and characterize this material in detail would certainly offer new possibilities to those interested in photonics and sensing applications. Many of the reported investigations in this area have been towards the synthesis of new materials under this motif. Less has been done for the understanding of the mechanism of energy transfer and excitation in such systems. Early studies on luminescent dynamics and other properties of lanthanide ions were primarily performed on inorganic matrices that cannot be easily varied on the molecular level [54]. Recently, lanthanide–organic composite systems have been used in the fabrication of near-infrared (NIR) electroluminescent devices for optical communication applications [55, 56]. One system which demonstrated impressive energy transfer efficiency properties was found and figure 2 shows the synthetic pathway for the creation of this lanthanide ion-cored dendrimer system. Here, a praseodymium ion was chosen as the core luminescent centre with conjugated chromophores attached as dendrons. The use of this type of topology permits the facile manipulation of the ligands at the molecular level, which allows the compound to fulfil the design criteria for a given application. Furthermore, an antenna effect (energy transfer) from the dendrons or metal-centred ligands to the core can originate a remarkably sensitized fluorescence of lanthanide cations within the lanthanide-cored cavity.

1.4. *Non-linear optical properties of dendrimer nanocomposites*

Dendrimer–metal nanocomposites have also demonstrated novel optical-limiting effects [47]. Both gold and silver metal–dendrimer nanocomposites have demonstrated this process at a variety of wavelengths as well as laser pulse durations [47, 57]. Owing to possible applications in eye and sensor protection the optical-limiting properties of dendrimer–metal nanocomposites offer new avenues toward the fabrication of solid-state devices with well-defined optical properties [58]. There has also been some interest in the understanding of the mechanism of the optical-limiting effects in these structures [59]. It has been suggested that 'localized' heating and subsequent bubble formation could be significant in the optical-limiting process in dendrimer–metal nanocomposites [47, 60]. This and other suggested mechanisms have been investigated both theoretically and experimentally, and in some cases the definite optical-limiting properties of DNCs have been compared to those observed in other well-characterized metal topologies [59]. An understanding of the connection of the metal topology with the topical limiting behaviour is best gained by closely analysing the dynamics of excitation and emission in metal nanoparticles in general. As it was found that the intrinsic linear and non-linear optical properties of different metal topologies are not the same [47, 57, 59], it is expected that the dynamics of excitation and emission should also vary with particle dimensions [48].

1.5. *Optical excitations in metal nanoparticles*

From the standpoint of optical excitations in dendrimer–metal nanocomposites, some researchers have been most interested in the mechanism of excitation and emission of the encapsulated metal particles. As it is well known in the case of semi-conductors, the conduction and valence bands are separated by a well-defined

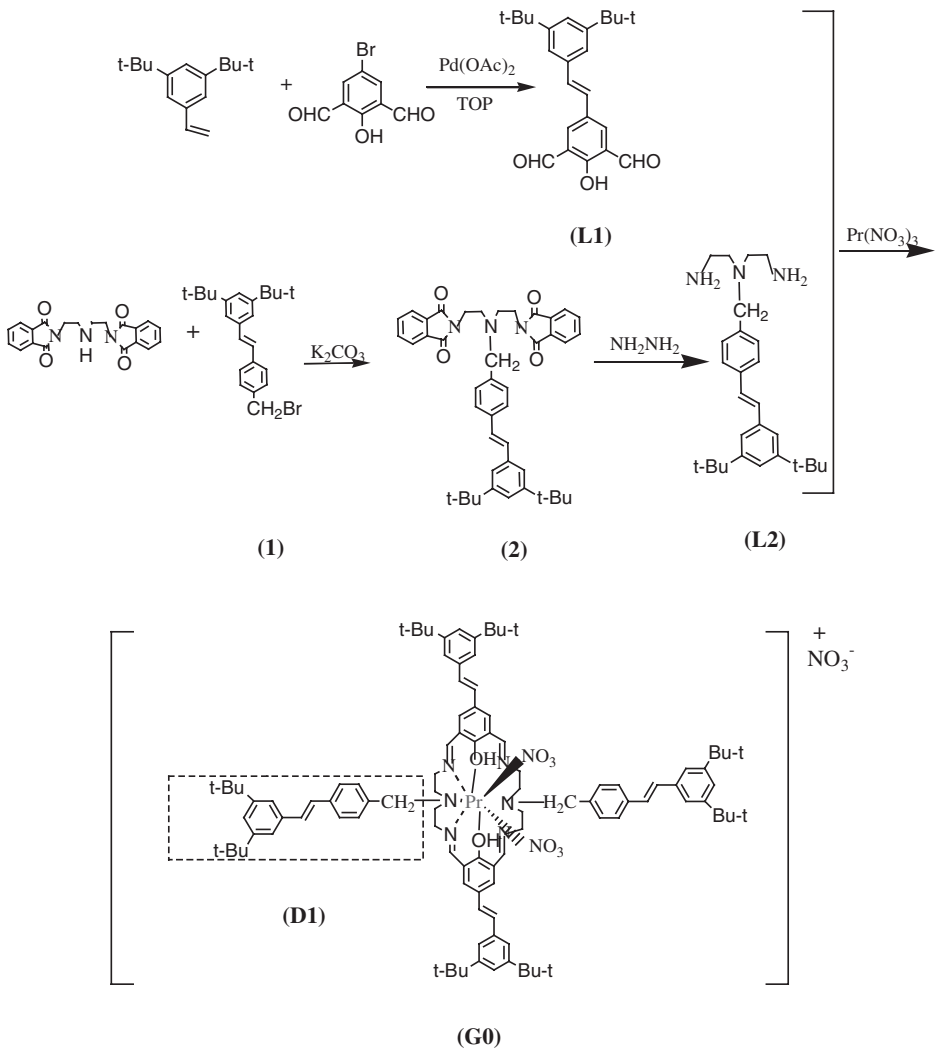

Figure 2. The synthetic scheme for the synthesis of a Pr lanthanide ion-cored dendrimer system. The conjugated stilbene units act as ligands/donors for energy transfer and other optical applications.

band gap. However, metal nanoparticles have half-filled the conduction band and the associated electrons are suggested to have the ability to move almost freely for particles as large as a few tens of nanometres [61–63]. When the particle diameter becomes smaller than the electronic mean-free path in the bulk metal (about 10 nm) the scattering of free electrons at the particle surface should be taken into account [63, 21]. For even smaller sizes (< 2 nm for gold) the phenomenological description of free electrons is anticipated to fail, as the fundamental assumption of infinite lattice periodicity and continuous energy-level spectrum is not valid any more [64, 65]. Such small clusters demonstrated a molecular type behaviour with optical properties very different from those for metal nanoparticles of bigger sizes [65]. In this review we focus on dendrimer–noble metal nanocomposites with metal particle sizes large enough to possess the main conductive electron properties of the bulk

metal. These conductive free electrons ultimately give rise to a surface plasmon band in the metal cluster's absorption, which depends on both the cluster size and the chemical, and in some instances biological, surroundings [66, 67]. The application of this property to dendrimer–metal nanocomposites has been the focus of a number of new optical uses involving photonics, biological sensing, as well as medical applications [68, 69]. For example, applications involving laser-induced optical breakdown have also been reported [60]. Here it was suggested that for biomedical systems, dendrimer nanocomposites can be biochemically targeted to sites where localized photodisruption can be induced, either by releasing encapsulated therapeutics or by ablating aberrant cells such as cancer cells or tissue [60, 70]. While this idea has been demonstrated for other metal-containing architectures involving organic macromolecules, the defined volume of metal particles encapsulated as well as the ability to tune the resonance may offer new opportunities in this regard [71].

In order to probe the fundamental excitations in these novel metal nanoparticle materials, it is important to understand the nature of the electron dynamics in metal particles in general. Electron dynamics in small metal nanoparticles probed by femtosecond transient absorption spectroscopy has been the subject of intense activity [72–75]. This method made it possible to monitor processes like electron thermalization [76], electron cooling and decay at high electron temperatures (see figure 3) [77]. For example, the thermalization time of an initial non-Fermi electron distribution in gold nanoparticles was estimated to be about 500 fs [78]. This is close to that measured in gold films by a similar method [76] or by photoelectron emission spectroscopy [79, 80]. Gold nanorods and nanospheres are two particular types of metal nanoparticles that have recently attracted great attention in investigations of particle shape effects on optical excitations [81]. Light scattering investigations

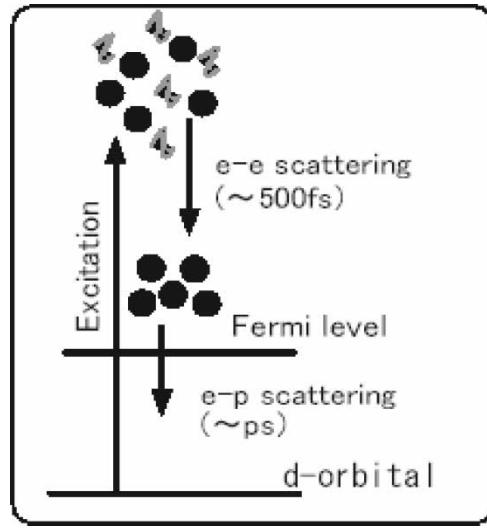

Figure 3. An illustration of gold photoexcited electrons relaxation in the time of picoseconds [181]. The electron–electron scattering process is caused by collisions of electrons within 500 fs and the e–p scattering process is caused by energy transfer to phonons during several picoseconds. Reprinted with permission from [181], copyright (2001) of the Japan Society for Analytical Science.

have been carried out with single nanorod particles and a 'drastic' reduction of the plasmon dephasing rate in the rods (in comparison to nanospheres) was observed [82]. The reason for this reduction was suggested to be due to suppression of interband damping for the longitudinal resonance [82]. There have also been reports on surface enhanced Raman scattering with metal nanorods [83] as well as on excitation of anisotropic coherent vibrational motions in such systems [84]. However, there have been only a limited number of reports on the time-resolved emission in gold metal particles [48, 57] and just one report of ultra-fast emission in gold nanorods [85]. All of these give details that are characteristic of different metal topologies, and are important in understanding the optical properties in the newly created dendrimer–metal nanocomposites.

The local field effect or local field enhancement is a very important aspect of electromagnetic field–metal nanoparticle interaction. Much attention to this effect was initially generated by the observation of an enormous enhancement of the Raman cross-section of the molecules absorbed onto a roughened metal surface, a phenomenon which has become known as surface-enhanced Raman scattering (SERS) [24, 86–88]. It is now widely accepted that the enhancement of an electromagnetic field close to a surface is responsible for the major part of SERS [88] (although a so-called 'chemical' effect can also contribute to SERS [89]). Near the metal surface the local field strength can greatly exceed that of the applied field due to excitation of localized surface plasmon resonances and shape ('lightning rod') effects [90, 91]. Depending on the material and the coupling between different surfaces, the enhancement of the local field can vary by several orders of magnitude [88]. The theory of local field enhancement has been developed by a number of authors to treat the specific surface optical process under consideration [90, 92–94]. In the simplest approximation, the enhancement of the local field near the metal hemispheroid can be given by the correction factor L, which describes the ratio of the macroscopic local field and the applied field [91]:

$$L(\omega) = \frac{L_{\mathrm{LR}}}{(\varepsilon_1(\omega) + i\varepsilon_2(\omega))/\varepsilon - 1 + L_{\mathrm{LR}} * \left(1 + (4\pi^2 iV[1 - \varepsilon_2(\omega) - i\varepsilon_2(\omega)]\varepsilon^{1/2})/(3 * \lambda^3)\right)} \tag{1}$$

where ε_1 and ε_2 are the real and imaginary parts of the dielectric constant of the metal, ε is the dielectric constant of the surrounding medium, V is the spheroid volume and λ is the wavelength. L_{LR} (lightning rod factor) is related to the spheroid geometry as a function of aspect ratio b/a:

$$L_{\mathrm{LR}} = 1 - \frac{\xi Q_1'(\xi)}{Q_1(\xi)}, \qquad Q_1(\xi) = \frac{\xi}{2}\ln\left(\frac{\xi + 1}{\xi - 1}\right) - 1, \qquad \xi = \left[1 - \left(\frac{b}{a}\right)^2\right]^{-1/2} \tag{2}$$

Along with the SERS, the local-field effect is responsible for the variety of other effects including the enhancement of the luminescence [26, 81, 95, 96], surface-enhanced second harmonic generation [94], and the increase of photochemical activity of adsorbates [97]. Owing to small sizes and possible complex shapes of the metal particles within the nanocomposites, the local field effects can strongly affect the optical properties of metal nanocomposites and, therefore, should be carefully accounted for in the theoretical and experimental investigations of the optical properties of these systems.

The details of time-resolved emission in metal nanocomposites and other metal topologies are important for they can lead to a better understanding of the enhancement process that is observed in different metal geometries, and may further lead to information regarding the actual mechanism of emission in gold particles. The two principal processes that may lead to emission in gold nanoparticles are: (1) direct (intraband) excitation of the surface plasmon resonance and emission from this collective electron motion [98, 99], (2) excitation of an interband transition followed by electron–d-holes recombination emission [81]. The second mechanism is enhanced by a strong local electric field in the vicinity of the longitudinal surface plasmon resonance for the case of gold nanorods [21, 81]. The strong non-linear optical properties and the enhanced optical emission in different metal topologies share a common characteristic of the dependence of a strong contribution on the surface plasmon resonance and the change in distribution of free electrons. Thus, reports have shown a strong correlation between the fast non-linear optical processes around the surface plasmon and electron distribution change and its dynamics [100, 101]. Alterations of the interband contributions to the dielectric function combined with the change of the interband absorption spectrum due to Fermi surface smearing are critical to this process. Understanding how these processes change with a particular size and shape as well as environment is very important. The shape and size of the metal clusters formed inside organic dendrimers are also parameters that strongly affect the emission properties [71]. Ultra-fast emission in gold– and silver–dendrimer nanocomposites suggests an emission process that is not unlike that observed in metal nanospheres and nanorods [85]. Here, it is also suggested that the dynamics of the emission process is dominated by a band-to-band transition with enhanced local field contributions [85].

1.6. *The focus of this review*

The purpose of this review is to report the current understanding and applications of a novel metal nanoparticle topology such as dendrimer–metal nanocomposites. This includes efforts to synthesize new guest–host dendrimer nanostructured materials with well-defined structure and composition. This also concerns the functionalization of the branching macromolecule with organic chromophores on the surface of the branching structure, which also holds the capacity to encapsulate metal nanoparticles. Furthermore, the synthesis and characterization of lanthanide ion centres are discussed as such systems constitute a very promising application for dendrimer nanocomposites. Many of these metal–dendrimer nanocomposites are normally characterized by their steady-state properties. Thus, the details and analysis of the surface plasmon absorption from metal particles in dendrimer nanocomposites are discussed. As we had discovered, certain dendrimer–metal nanocomposites possess impressive optical-limiting properties in nanosecond green light laser pulses [47]. This process is important for the creation of devices for eye and sensor protection. The mechanism and analysis of the enhancement of the optical-limiting behaviour in certain DNCs in comparison to other metal topologies are important issues. As stated above, another major emphasis of our group has been to characterize the dynamics of emission in DNC systems. A close analysis of the dynamics of emission from pure (micelle) metal topologies is given first. This is used as a comparison with the dynamics and magnitude of the enhanced emission observed in dendrimer–metal nanocomposites. Close analysis of the dynamics of emission of the dendrimer–metal nanocomposites under different environmental

conditions provides important information regarding the future use of the dendrimer nanocomposites materials in biological (water soluble) and medical technological applications. This and other possible future directions for optical applications and fundamental investigations are presented in this review.

2. Synthesis and fabrication

2.1. *Background of fabrication of metal nanoparticles*

The synthesis and characterization of transition metal topologies have enjoyed great success in a number of different scientific areas. As stated above, gold particles of nanometre size have been synthesized by using surface-active molecules as stabilizers. While other reviews have presented full details of the fabrication of metal topologies from micelles and other surface-active molecules [21], in this review we will focus on the creation and optical properties of dendrimer–metal nanocomposites. Since the first report of a poly(amidoamine) (PAMAM) dendrimer system encapsulating a metal nanoparticle, different nanocomposite systems have been prepared by incorporating both large and small nanoparticles, as well as by using large and small dendrimer macromolecules [33–41]. Metals such as gold, platinum, silver, palladium and copper have all been used in this structure. As is often the case when considering the creation of such structures, great emphasis is put on the characterization of the composite materials. Characterization techniques such as transmission electron microscopy (TEM) [102], UV–Vis absorption [47, 48], mass spectrometry [103], as well as electrochemical [104] and chemical (stoichiometry) [105] methods have been used in support of the reported nanocomposite architectures.

2.2. *Synthesis of metal nanospheres and nanorods*

Before describing the synthesis and fabrication of metal particles encapsulated in dendrimers, it is important to briefly discuss some of the basic metal particle topologies formed initially by other well-established methods. As stated above, the creation of metal topologies by micelle structures has been well documented in the literature [21]. For example, considering the comparison of the optical excitations in dendrimer–metal nanocomposites in this review, it is important to examine the formation of different metal particles with distinct aspect ratios. In particular, gold nanospheres (SP) have been created under an electrochemical methodology and can show a wide variety of diameters. Additionally, gold nanorods of different aspect ratios may also be prepared in micellular form as outlined in the literature [21]. These systems are soluble in aqueous solution at room temperature. TEM measurements have been extensively used to characterize the size and distribution of these and other nanoparticle topologies. In the case of gold nanorods, an enhancement of the emission by a factor of 10^6 has been observed. Other novel nanoparticle systems such as cadmium sulphide have also been prepared [106]. Pelini *et al*. [107] have investigated interesting silver nanodisks and gold nanoboxes as well. While it is not the aim of this review to discuss all the established methods of fabricating metal nanoparticles, it is important to note that from the extensive literature regarding this it is possible to compare and correlate certain characteristics observed in these nanoparticle systems with those found in dendrimer nanocomposites as shown below.

2.3. *Initial fabrications of dendrimer–metal nanocomposites*

The fabrication of dendrimer–metal nanocomposites has been carried out using a number of methodologies. In many ways these synthetic methods for creating DNCs are fairly direct and allow for the use of different approaches to a common goal. Many of these methods have employed poly(amidoamine) (PAMAM) dendrimers as host of the metal nanoparticles [33, 34]. Nowadays, a variety of PAMAM dendrimer generations are commercially available [108]. The host PAMAM dendrimers can be tailored with the appropriate functional groups (on the surface or interior) for further chemical alteration. The host PAMAM dendrimers have either amine functional groups or a COOH group that can be functionalized on the surface [109, 110]. The fabrication method varies depending on the different type of architecture desired, and on the different metals. However, the main procedure requires the host dendrimer to be initially charged (see figure 1). The charged dendrimer is then added to the appropriate metal salt to form a complex. The particles are consequently formed by the addition of a reducing agent such as $NaBH_4$. The rate of reduction, dendrimer size (generation), weight ratio and concentration of dendrimer are all important parameters in the fabrication of the dendrimer nanocomposites. The type of metal is also very important in the fabrication of the particles. Crooks *et al.* [111, 104] demonstrated that metal nanoclusters ranging in size from 1 to 2 nm could be prepared within dendrimer templates by a two-step synthesis process. It was found that the Cu clusters were initially formed in the interior of certain PAMAM (–OH terminated) dendrimers. The Cu clusters are then displaced by Ag, Au, Pt or Pd nanoparticles and the remaining Ag nanoparticles can be exchanged with Au, Pt and Pd as well (figure 1C) [104]. More recently, monodisperse Pd nanoparticles have been prepared by another two-step process that involves first, the formation of a nanoparticle inside the dendrimer and then, the extraction of these particles from Pd dendrimer nanocomposites by *n*-alkanethiols [111].

Other literature reports [43] have shown that the nanocomposite preparation procedure is partitioning of a particular number of metal ions into the dendrimer's interior. The success of these chemical reactions is suggestively due to associative properties of amines or other terminal groups. It has also been reported that dendrimer-encapsulated metal nanoclusters can undergo multiple *in situ* displacement reactions [104]. The dendrimer nanocomposites encapsulated Pd and Pt nanoparticles prepared by direct reduction [43], and by primary or secondary displacement reactions [104], are catalytically active for electrochemical reduction of O_2 [112]. These structures were characterized by TEM, X-ray photoelectron spectroscopy, as well as UV–Vis spectroscopy [112]. With precise functionalization, it may be possible to prepare different types of dendrimer nanocomposite architectures. Balogh and Tomalia have used the functionalization of PAMAM dendrimers to create external and internal dendrimer nanocomposite structures [113, 114]. They suggested that the dendrimer hosts are monodisperse nano-reactors, possessing the architecture and ligand sites that allow the preorganization of metal ions within their interiors. It was also reported that the use of PAMAM dendrimers as templated containers allows '*in situ*' generated reaction products to be dispersed as amorphous or slightly ordered domains within the dendrimer interior [114]. Several interesting applications have been suggested given the flexibility of the synthesis in this manner, including encapsulating semi-conductors, noble metals, environmental cleanup, as well as magnetic and electronic applications [1].

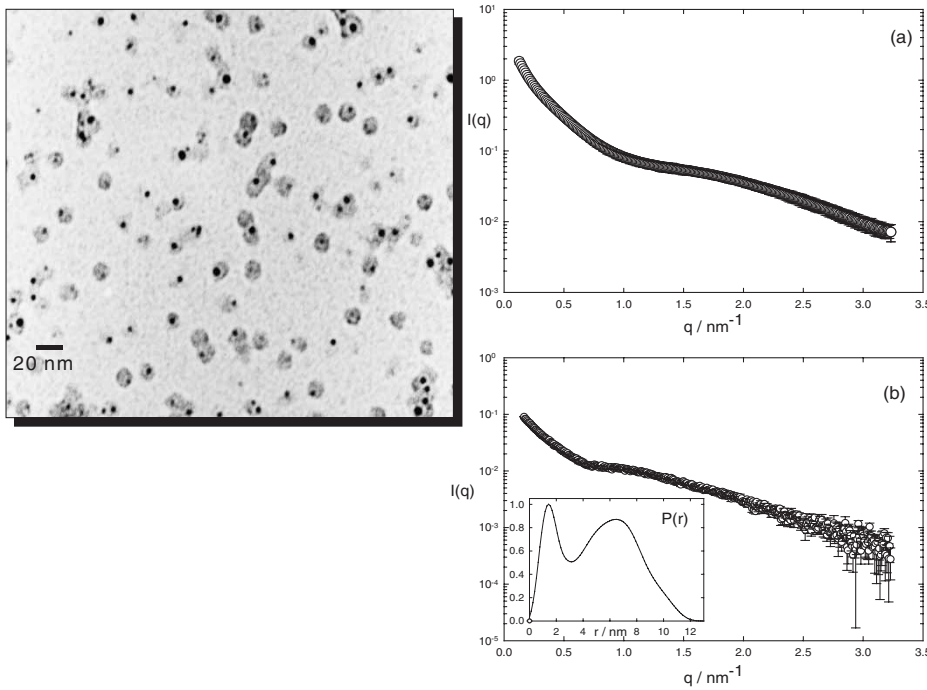

Figure 4. TEM (left) for PAMAM G9 dendrimer nanocomposites [102] and SAXS of gold nanocomposites with PAMAM dendrimers of (a) the fifth generation NG5, and (b) the ninth generation NG9 [71].

2.4. *Fabrication of dendrimer–metal nanocomposites with different morphologies*

Some reports have devoted great attention to the characterization of the formed nanocomposites. In a report by Amis and Bauer, several generations (from G2 to G10) of PAMAM dendrimers were used as potential nano templates for the formation of inorganic–organic hybrid colloids in aqueous solution [102]. The reduction of gold with sodium borohydride was used in the synthesis, since it was previously shown that the reaction speed could be controlled. While it was not reported that $AuCl_4^-$ ions exhibit any specific coordination to amine groups, it has been shown with polyelectrolyte microgels that $AuCl_4^-$ has sufficient electrostatic attraction of precursor ions to form inorganic–organic hybrid structures. The different structures formed with the diverse dendrimer–metal combinations were characterized by TEM and SAXS (see figure 4) and found to be very inclusive of several different types of structures [102]. Gold/dendrimer ratios, as well as dendrimer mass fraction, and reaction rate are all important in determining the desired structures. It was also found that under certain experimental conditions PAMAM dendrimers in the range of G2 to G4 may behave like molecular mass colloid stabilizers. The suggestion for these systems is that several dendrimers surround the surface of the metal particles formed. The higher generation systems were found to be very different for several cases. For G6 to G9, the PAMAM dendrimers act as effective 'polymeric' templates [102]. Metal particles are completely formed inside individual dendrimers (figure 4). The metal particle was shown to be somewhat off centre inside the dendrimer host. This work demonstrated that the size of the inorganic colloid can be precisely con-

trolled by the number of precursor ions added per dendrimer molecule; and this may be done without changing the morphology of the hybrid particle.

The action of a template synthesis has also been reported for different dendrimers and different generation numbers. Bauer *et al.* [71, 102] have fabricated and characterized DNCs of generation 5 and 9 (NG5 and NG9 in their notation) [71]. In the case of the NG5 the loading ratio was of 1:1 in terms of gold ions per dendrimer surface groups. For the NG9 the loading ratio was about 1:2. For generation 9, from TEM and SAXS measurements the gold particle diameter is found to be 3.2 ± 0.2 nm [102]. This diameter corresponds to that expected for 'fixed loading', i.e. formation of one gold cluster consisting of 1024 atoms. For the NG5 sample a 'fixed loading' would imply 128 gold ions forming a single particle of 1.6 nm in diameter. However, they observed an average diameter larger than expected for fixed loading for the metal particles (associated with the aggregated dendrimers) formed with G5 dendrimer. These results suggest that the sample is at a transition between the 'stabilizing' and the 'templating' mechanism of colloid formation [71]. In addition to the loading ratio, another important factor concerning the two samples investigated here is the concentration of their preparation. The initial concentration of dendrimers in the solution was about 0.14% (mass fraction dendrimers in H_2O) for the NG9 and about 0.33% for the NG5. The lower concentration, applied for the NG9 sample allows the dendrimer to act as true template and thus the formation of well-defined hybrid particles. In contrast, particle formation at higher concentration had led to less defined nanoparticles, e.g. higher polydispersity [71, 102].

2.5. *Synthesis of chromophore–PAMAM dendrimer nanocomposites*

The optical properties of PAMAM dendrimers appear to be intrinsically interesting [115, 116]. However, they are not the focus of this review. It is important to note that when chromophores are attached to the surface of dendrimers and metal nanoparticles, new properties and questions arise [59, 111–122]. For example, using PAMAM dendrimers bearing multi-chromophores on the periphery could possibly enhance fluorescence emission. Since functionalizations are performed by attaching fluorescent chromophores on the external surface of the dendrimers, a well-defined number of chromophores in a confined volume element can be obtained and easily controlled [120]. Other functional groups such as specific receptors, antibodies, ligands, even DNA itself can couple or possible form complexes with the partially functionalized dendrimers [123, 124]. Such multi-functional architecture may be the basis for their application as sensors, affinity assay components, and in fluorescence imaging in cell biology. The non-linear optical building blocks can be also placed at the periphery of the dendritic scaffold to enhance non-linear optical effects [59]. Furthermore, anionic starburst dendrimers have been used as templates for investigation of the adsorption and aggregation of organic dyes. Kaifer *et al.* [120] used a variety of molecular and ionic quenching measurements to assess the relative structural permeability of a single pyrenyl residue attached to the tertiary amino within a series of asymmetric PAMAM dendrimers possessing carboxylate moieties on their periphery. From their quenching measurements, chain segmental densities and pyrene accessibility are probed as a function of dendrimer generation number provided insight in the role of size and electrostatics in this process. Stern–Volmer behaviour was observed during the different quenching experiments carried out with their system. Balzani *et al.* have also prepared chromophore-functionalized dendritic architectures for the purposes of light-emitting and -sensing applications [122].

Motivated by these potential applications and attractive fundamental questions concerning macromolecular structure functionalization, there is significant interest in the fabrication and characterization of novel functionalized dendrimer structures.

In many cases, the quenching and enhancement of metal emission from organic chromophores by metal particles have been also theoretically considered. Quenching by Förster transfer to the surface plasmon absorption of the metal has been well described in the literature [26]. This is strongly dependent on the distance between the metal surface and the chromophore [96, 125] and on the metal nanoparticle size as well [126]. In a very general model one may simply consider the effect on the fluorescence quantum yield which can be understood by the relationship [96],

$$Y = \frac{\left|L(\omega_{\mathrm{flu}})\right|^2}{Q_{\mathrm{o}}\left|L(\omega_{\mathrm{flu}})\right|^2 + Q_{\mathrm{o}}A(\xi - \xi_{\mathrm{o}})^{-3} + (1 - Q_{\mathrm{o}})} \tag{3}$$

Here $L(\omega_{\mathrm{flu}})$ corresponds to the local field factor (see equation (1)), Q_{o} is the initial quantum yield of fluorescence of the organic chromophore without the presence of the metal particle, the ξ terms describe the distance between the two components and A is an amplitude term. The use of this expression can be considered in limiting cases that are related to the initial quantum yield of the dye and distances from the metal. As for intermediate distances and small Q_{o} the expression leads to a limiting value of $1/Q_{\mathrm{o}}$ for enhancement [96, 92]. While there are still important parameters to be determined from the precise manner in which the rate and quantum yield change in this process, it is certain that the enhanced field and increased radiative rates occur at longer distances from the metal than quenching. Thus, it is predicted that in the region between 5 to 20 nm from the metal surfaces the emission of chromophores may be enhanced [96].

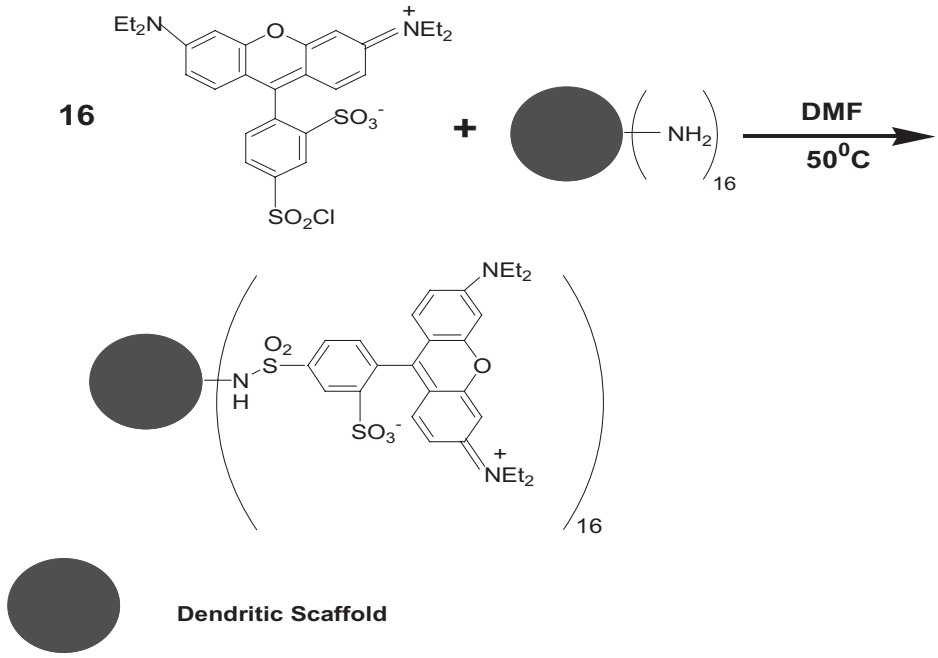

Figure 5. Schematic diagram of the synthesis for the rhodamine-functionalized dendrimer.

We have functionalized a starburst PAMAM dendrimer G2 by a rhodamine chromophore (see figure 5) [127]. This functionalized dendrimer has been used as a template or stabilizer to encapsulate gold nanoparticles. The fluorescence dynamics of this dendrimer, model compound and the gold nanocomposites were compared. A rising time and a fast component in G2–LRSC system indicate strong interactions among peripheral chromophores. The encapsulation of gold nanoparticles leads to disappearance of the rise time and the faster decay compared to G2–LRSC, suggesting the strong interactions occurred through the energy transfer from dendritic chromophores to metal nanoparticles. The gold nanoparticles strongly quench the steady-state fluorescence of G2–rhodamine (G2–LRSC). From the discussion above, it is clear then that in this case of the chromophore-functionalized dendrimer–metal nanocomposites (G2–LRSC–Au) the encapsulated metal nanoparticles are too close to the chromophores for enhanced emission to be observed.

PAMAM dendrimers are not the only host branched structures used to prepare metal nanocomposites, and there have been a number of different structures used for the purpose of encapsulating metal nanoparticles. For example, Fox *et al*. [117] have devised novel synthetic routes where new nanoparticle-cored dendrimers were prepared by the reduction of hydrogen tetrachloroaurate phase-transferred into toluene in the presence of Fréchet-type polyaryl ether dendritic disulphide wedges of generation 1–5. These gold-cored dendrimer nanocomposites are radially connected by Au–S bonds that occurred through nanometre-sized gold clusters at the core and dendritic wedges. The structures of these nanocomposites are well characterized by TEM, TGA, and steady-state spectra [117]. Müllen *et al*. [118] have also prepared metal nanostructures using a stiff polyphenylene dendrimers functionalized with 16 thioethyl groups on the outside. They used dendrimer-controlled 'one–pot' synthesis of gold nanostructures [118], and a bimodal particle size distribution was observed. The small nanoparticles are subjected to aggregation in the solid state due to the cross-linking ability of the dendrimer. The gold–dendron nanocomposites have been fabricated by use of poly(oxymethyphenylene) dendrons of generation 1–4 functionalized with a thiol group at the focal point as a capping ligand [119]. Using this particular method fairly small particles (~1.5 nm) could be consistently prepared [119].

2.6. *Synthesis of lanthanide ion-cored dendrimer composite*

The unique optical properties of lanthanide ions (Ln^{3+}) have contributed to the development of a number of applications such as photoluminescence and electroluminescence materials, laser sources, and optical amplifiers. For those applications, one needs to dope lanthanide ions into polymers, sol–gel, or inorganic crystal and inorganic nanoparticles. To overcome the poor solubility of lanthanide salts in polymer matrices and in inorganic media, two methods were used for the fabrication of polymer-based lanthanide composites. One is to dope an organic cage-like complex that encapsulates the Ln^{3+} into the polymer, the other is to combine the Ln^{3+} that was hosted by the excellent properties of SiO_2 with the easy processing of polymer [128]. The attachment of highly absorbing sensitizers, such as lissamine [128], fluorescein, eosin, and erythrosine [129], and porphyrin [130] to the complexes can sensitize the NIR emission of lanthanides and solve the problem of using very high powers to achieve population inversion. However, the lower quantum efficiency is an intrinsic problem for the polymer systems that doped organic complexes. The solving of photostability of dyes and optimization the preparation SiO_2–Ln^{3+}–

polymer nanocomposite may make these materials a reality for optically pumped lanthanide-doped polymer amplifiers.

The blend of conjugated polymer with dye-functionalized lanthanide complexes provides an opportunity to use these composites to fabricate an electrically pumped polymer waveguide amplifier operating in the near infrared. Lanthanide complexes with π-conjugated ligands such as β-diketonate, bipyridine, etc., have also been synthesized for the emitting layer in electroluminescence devices that emit visible light [52]. Recently, great efforts have been devoted to the synthesis of dendrimer-based lanthanide composites for preventing self-quenching and improving the heterogeneous dispersion of lanthanide ions in the polymeric and inorganic matrix. We have synthesized a praseodymium ion-cored dendrimer composite (see figure 2) and investigated the optical properties of this system. It was found that the line emission of Pr^{3+} resulted from very efficient energy transfer from the dendrons to metal centre [131]. Frěchet *et al.* [132] also prepared lanthanide ion-cored dendrimer composites, which consist of Ln^{3+} (Er^{3+}, Tb^{3+}, and Eu^{3+}) cores and a surrounding dendritic carboxylate shell. These systems show an enhancement of the lanthanide ion emission through site-isolation and antenna effects. An amphiphilic copolymer synthesized from hydrophilic block poly(acrylic acid) and hydrophobic block polyether dendron can encapsulate Tb^{3+} and possibly self-assemble into micelle-like aggregates in aqueous solution. Therefore, the enhancement of luminescence has been attributed to both the microenvironment and antenna effects [133]. Furthermore, Yamashita *et al.* synthesized a new type of dendritic macromolecule as functionalized ligands for encapsulating Gd^{3+} [134]. In the case of the lanthanide dendrimer mentioned above, the antenna effects are not particularly efficient as sensitizers for lanthanide emission, therefore, a phosphinoxide ligand that possesses strong binding properties and excellent sensitizing capabilities has been synthesized to complex lanthanide [135]. Recently, Balzani *et al.* [136, 137, 49] synthesized dansylated dendrimers to encapsulate lanthanide ions. Such composites have been used to study the antenna-like sensitization of visible and near-infrared emission of lanthanide ions.

3. Optical methods

3.1. *UV–Vis absorption measurements*

Perhaps the most common manner in which the different metal nanostructures have been characterized is through their UV–Vis spectra [21, 57, 138], as it is the measurement of the surface plasmon resonance (SPR) band that sheds light on: (a) the identity of the metal particles [139] or particles' array [140], (b) the existence of a metal particle 2 nm or larger in size [21, 102], (c) the shape or aspect ratio of the metal particle [21, 81], and (d) in some cases the size distribution of the metal particles. Different particles show distinct surface plasmon resonance. For gold particles (2 nm or larger) the resonance is near 520 nm [21], for silver it is near 440 nm [106], and for copper it is at 625 nm [17]. The significant optical density of the SPR is a good measure of the approximate extent of particle (colloid) formation. For metal particles with different aspect ratios, a longitudinal plasmon resonance is observed [21, 81, 85]. This occurs in general at lower energies (depending on the diameter and length of the particle) from the transverse resonance. In some cases, particularly for the larger particles formed in PAMAM dendrimers, the width of the SPR can give information on metal aggregates with complex shapes [48, 71]. This is not in any way

a substitute for more sensitive measurements of distribution such as TEM, SAXS (see figure 4), and SANS.

However, the best option for characterization of these systems is to use optical measurements such as UV–Vis absorption in combination with sensitive microscopy and scattering techniques, to obtain a clear picture of size distribution and the shape of prepared nanoparticle systems.

3.2. *Steady-state emission*

While it is known that the steady-state emission efficiency of pure bulk metal is small ($\sim 10^{-10}$) [141], new particle shapes and properties have suggested significant enhancement of the quantum yield [21]. In metal nanorods, El-Sayed has reported enhancement of the steady-state emission on the order of 10^6, which gives rise to easily observable emission spectra [81]. The suggested mechanism is due to local field enhancement [81]. In metal–dendrimer nanocomposites (gold and silver particles inside dendrimers of sizes larger than 2 nm) the enhancement factors have not been so significant as to allow the emission to be observed by conventional steady-state spectroscopic methods [48]. While relatively small contributions of steady-state emission have been reported for the case of the pure PAMAM dendrimer or residual emission in the nanocomposite due to the PAMAM host [115, 116, 142], this method seems to be most appropriate for metal particles with significantly larger aspect ratios and larger enhancement factors.

3.3. *Non-linear transmission measurements*

Dendrimer–metal nanocomposites demonstrate novel optical-limiting effects that can be examined by non-linear transmission measurements [47, 59]. Laser excitations and energies that are particularly relevant to the applications involving eye and sensor protection use ns pulses of green light. For example, for the measurements of the non-linear transmission effects in these novel gold nanostructures, a non-linear transmission apparatus with similar parameters to those reported in the test beds of other interesting optical-limiting materials were reported [59]. A Nd:YAG laser operating at 1064 nm (or at 532 nm using second harmonic unit) with a pulse duration of ~6.5 ns and 10 Hz repetition rate is generally used [47]. Many of the measurements were carried out at 532 nm since this allows direct excitation of the transverse absorption resonance in the gold or silver nanostructures. The laser beam is focused with a $\sim f/25$ lens in order to produce a beam spot of ~40 μm in diameter. The sample is positioned in the focal plane [47, 59]. Two photo-diode detectors are commonly used for the reference input and transmitted output intensities. The output photo-diode is placed away from the sample. A boxcar integrator and associated electronics is commonly used to collect and analyse the transmitted light.

3.4. *Pump–probe transient absorption measurements*

As mentioned above, the relaxation of the optical excitations in metal particles involve many different processes, which occur on different time-scales. This requires the use of fast dynamics measurements of the excitations such as in the case of pump–probe transient absorption measurements. As there have been a number of reports of pump–probe measurements in gold and silver metal particles [143–147], the use of this technique has been well documented in the literature [143–147]. For the case of metal–dendrimer nanocomposites, pump–probe measurements have also been carried out with amplified pulses in the visible and near IR spectral regions

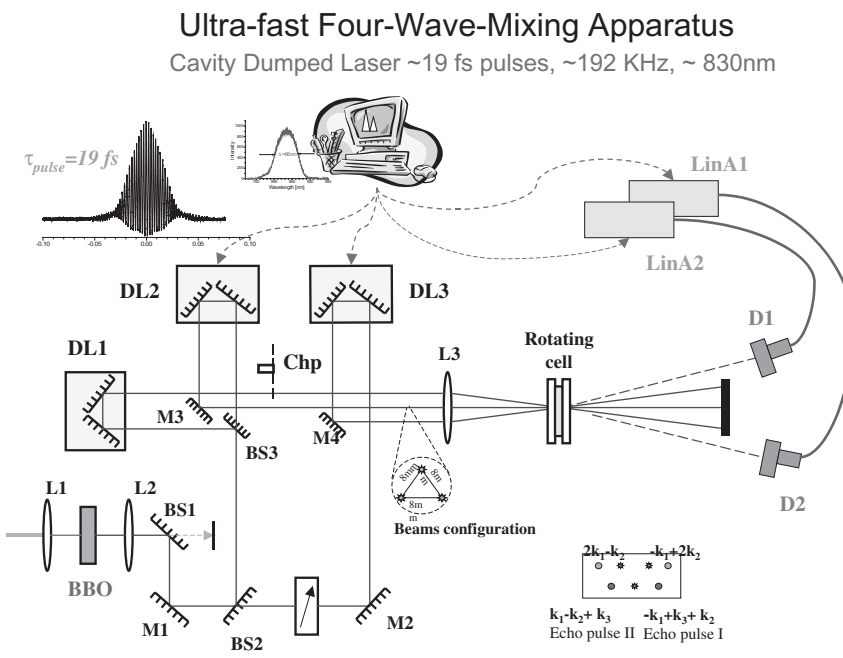

Figure 6. Pump–probe and three-pulse photon echo setup.

[148]. Recent pump–probe transient absorption measurements in DNCs have been carried out using a cavity dumped Ti:sapphire laser system, which was spectrally centred at 830 nm with a repetition rate of 192 kHz and 20 fs pulse width (see figure 6) [149]. The fundamental is passed through a non-linear BBO crystal and the second harmonic is generated which is then split into pump and probe beams using a beam splitter. Pump pulse energy is below 0.5 nJ where as probe pulse has energy ≤ 0.05 nJ. The pump beam was chopped using an optical chopper at a rate of 1.067 kHz (an optical chopper was synchronized to a locking amplifier) and focused on to the sample cell using a 10 cm lens. The probe beam is passed through an optical delay line and a 10 cm lens, and then it is overlapped with the pump beam in the sample cell and is detected at the photo-diode. Modulations in the probe beam with respect to the chopper are measured with the use of a lock-in amplifier and this signal is recorded as a function of the delay line on a PC. The width of the instrument response function is 60 fs.

3.5. *Fluorescence upconversion measurements*

Because of the very inefficient emission in dendrimer–metal nanocomposites continuous wave (CW), emission measurements give very little information about the excitations and dynamics in these systems. However, with ultra-fast time-resolved measurements it is possible to observe the very short-lived excited states in dendrimer nanocomposites [48, 57]. Recently, femtosecond upconversion spectroscopy was employed to temporally resolve the fluorescence and its polarization of the metal–dendrimer nanocomposites (see figure 7). The optical arrangement for a typical fluorescence upconversion experiment has been reported in the literature [150, 151]. For the measurements with the dendrimer nanocomposites the laser source was a

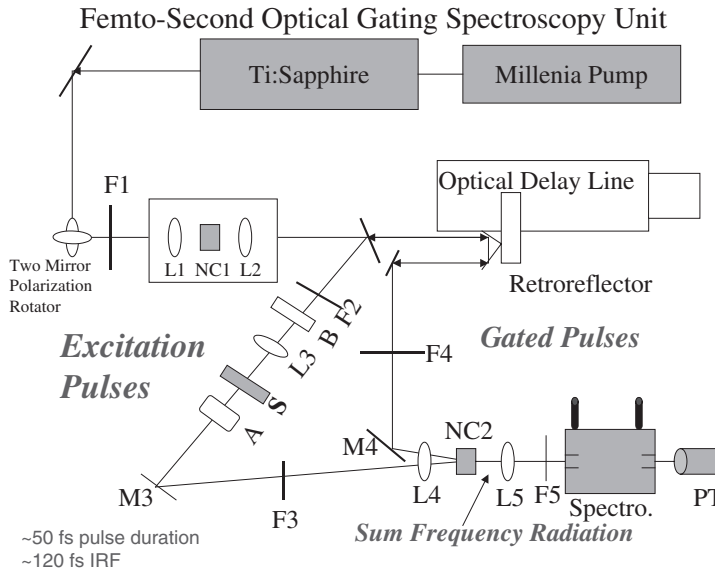

Figure 7. Fluorescence upconversion setup.

Ti:sapphire laser with an average pulse width of 70 fs tuned at 790–860 nm, and a repetition rate of 82 MHz (Tsunami, Spectra Physics). The sample was excited with light pulses delivered by the frequency-doubled output of the laser at 395–430 nm. The fluorescence emitted from the sample was focused with an achromatic lens into a non-linear crystal made of beta-barium borate (BBO). A temporal profile of the fluorescence was monitored by sum-frequency generation with the reference pulse from the laser at 790–860 nm that was first passed through a variable delay line. Sum frequency light was dispersed by a monochromator and detected by a single photon counting system. The time resolution was determined by the pulse width of the laser and group velocity dispersion within optical elements of the system [152]. The FWHM of the cross-correlation function at 790/395 nm was estimated to be 190 fs. It is important to note that we could observe the fluorescence dynamics on the time scale covering almost 4 decades (200 fs–1 ns) in one measurement. The rotating sample cell and holder (1 mm thickness in the case of solutions, ~1 μm thick in the case of thin films) were used to avoid thermal and photochemical accumulative effects. The excitation average power was kept at a level of a few mW. We found that there was no excitation intensity dependence of the decay dynamics when input powers were below 10 mW. The energy of the excitation pulse did not exceed 0.5 nJ/pulse. The measured fluorescence decay curves were fitted by the result of the convolution of the instrument response function with an exponential decay model in order to minimize the sum of weighted residuals (χ^2). The quality of the fit was monitored by the values of the reduced χ^2, the inspection of the residuals, and the monitoring of the auto-correlation function of the residuals. For low-temperature measurements we used an Oxford instrument with continuous flow He cryostat, which was interfaced (optically and electronically) to the upconversion unit [152].

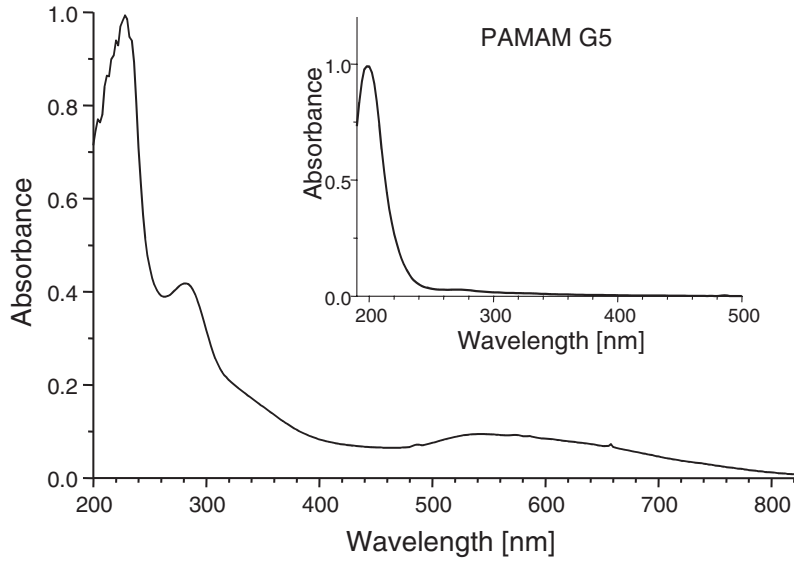

Figure 8. Absorption spectrum for the gold–dendrimer nanocomposite. Inset: absorption spectrum for PAMAM dendrimer (generation 5).

4. Steady-state properties

4.1. *Linear absorption in gold– and silver–dendrimer nanocomposites*

Linear optical absorption has been used to characterize the metal particle morphology in the case of gold– and silver–dendrimer nanocomposites [33, 47, 48, 57, 59]. Shown in figure 8 are the linear optical spectra for the Au dendrimer nanocomposite as well as the pure PAMAM dendrimer (generation 5). The absorption of the pure PAMAM dendrimer has a maximum at 230 nm. The absorption of the highly concentrated aliphatic amine groups is very strong. For comparison, the absorption spectrum of the dendrimer nanocomposite is normalized to unity. The surface plasmon resonance is clearly seen for the gold–dendrimer nanoparticles with a maximum at 530 nm. The FWHM of the surface plasmon for this particular dendrimer nanocomposite sample was ~80 nm [71]. It was found that the width of the surface plasmon changes with the particular dendrimer nanocomposite architecture. Silver–dendrimer nanocomposites have also been prepared and show a surface plasmon resonance at wavelengths shifted to the blue of the gold systems, as expected.

4.2. *Metal particle size and linear absorption*

As stated above, there is a connection between the size of the particles and the character of the surface plasmon resonance [21, 59]. The electric field of an incoming light wave induces a polarization of the 'free' conduction electrons with respect to the much heavier ionic core of the spherical nanoparticle [153]. The net charge difference occurs at the nanoparticle boundaries (the surface) which in turn acts as a restoring force. In this manner a dipolar oscillation of the electrons is created within a particular time period [153]. It was shown by Mie [154] that a series of multipole oscillations may be responsible for the extinction cross-section of metal nanoparticles [139, 154]. For nanoparticles much smaller than the wavelength of light, only the dipole oscillation contributes significantly to the extinction cross-

section. For larger nanoparticles the dipole approximation may no longer be valid, and the plasmon resonance will depend explicitly on the particle size [155]. The larger the particles become, the more important the higher order polar contributions. The plasmon bandwidth increases with increasing particle size.

4.3. *Linear absorption in other dendrimer–metal nanocomposites*

For other metal–dendrimer nanoparticles, such as those made of Pt^{2+}, (figure 1(c)) strong absorption in the ultraviolet has been observed [104]. Crooks *et al.* [43] have investigated changes in the linear absorption spectra of $PtCl_4^{2-}$ and its addition to G4–OH PAMAM dendrimer. When the two are mixed for sufficient time a new band at 250 nm is formed. This band was interpreted as being proportional to the number of Pt^{2+} ions in the dendrimer, with the number of atoms ranging from 0 to 60. In this case, the titration-like behaviour also suggests that it is possible to control the dendrimer–metal ratio [43]. The linear absorption spectra were also used to show that Pt particles arising from Pt^{2+} ions bound to the terminal primary amine ligands agglomerate, and only the intra-dendrimer bound Pt^{2+} ions yield stable soluble clusters. Crook's absorption results support the suggestion of the very high degree of stability in these dendrimer nanoparticles, in that no agglomeration was detected for up to 150 days and the material could be re-dissolved after repeated drying.

The linear absorption of dendrimer nanocomposite thin films has also shown interesting features. Tripathy *et al.* [156] have used the processes of electrostatic multi-layer deposition to form thin films of gold–dendrimer nanocomposites mixed with layers of poly(sodium 4-styrenesulphonate) (PSS). UV–Vis spectra of PSS/gold–dendrimer nanocomposites showed that in the UV region of the spectrum the amplitude of the absorption increased with increasing number of bi-layers. For these thin films the absorption of the gold could be monitored by UV–Vis spectroscopy as well. The number of cycles of adsorption was critical in observing the surface plasmon resonance [156]. The UV data suggested that the gold–dendrimer nanocomposite could be adsorbed onto the PSS film after a certain number of cycles had been completed. A uniform array of the gold–dendrimer nanocomposite on the PSS layer was further confirmed by AFM studies.

4.4. *Linear absorption and other techniques used in combination*

Some more recent reports have combined the use of linear absorption in dendrimer nanocomposites with other techniques sensitive to the particle's structure. For example, SAXS characterization of dendrimer–gold nanoparticles NG9 and NG5 (generation 9 and generation 5) has been carried out [71, 102]. An upturn at small q indicated an aggregated structure of the generation 5 sample. For this system the SAXS data revealed a radius of gyration of the hybrid particles (aggregates of dendrimers with associated gold) of $r_g = 7.5$ nm as compared to $r_g = 2.5$ nm for the initial G5 dendrimer. In contrast, for the generation 9 sample the SAXS suggested a layered sphere structure with a total diameter of 13 nm. This confirmed the suggestion that gold particles of 3.2 nm diameter are formed inside individual G9 dendrimer molecules. Modelling showed that the gold particles are located off-centre inside the spherical dendrimer molecule. It should be noted again that the dendrimer molecule does not have a hollow interior *a priori* but behaves like a 'homogeneous sphere' of dendrimer swollen with water [157]. Upon particle formation, parts of the dendrimer molecule can rearrange and some of the water is replaced by the gold colloid formed [158]. In this particular case the volume of the pure dendrimer was

about 750 nm^3 and the volume of water inside the dendrimer was about 1150 nm^3. The calculated volume of gold particle was about 17 nm^3 [71]. The absorption of the G9 system was very different to that obtained for the G5 sample. The generation 9 sample only showed a very small sloped absorption peak near 520 nm, suggesting that very small metal particles had formed in the host dendrimer. However, for the generation 5 system, a very broad and intense absorption band near 520 nm was observed. This may be due to the larger distribution of particles formed with the generation 5 system. Indeed, reports of this nature point out the important and necessary details and characteristics of dendrimer nanocomposites that are useful for optical and biological applications.

5. Non-linear absorption properties

5.1. *Non-linear absorption properties in silver–dendrimer nanocomposites*

It is now generally accepted that optical-limiting materials in the visible spectral region with broad non-linear spectra and short response times are required for eye protection and switching applications [159]. While the search for superior optical materials has enjoyed a long history of successful activity, there has been recent interest in the use of semi-conductor and metal clusters for this same purpose [160–162]. Different metal topologies have shown good optical-limiting behaviour where in some cases a size-dependent effect was observed. It was found that for particular size gold particles, the fluence threshold of the limiting effect decreases and its amplitude increases with increasing particle size. The first report of the non-linear optical properties of these novel nanocomposites was investigated with 6.5 ns laser pulses from a frequency doubled Nd:YAG laser at 532 nm [47]. The repetition rate

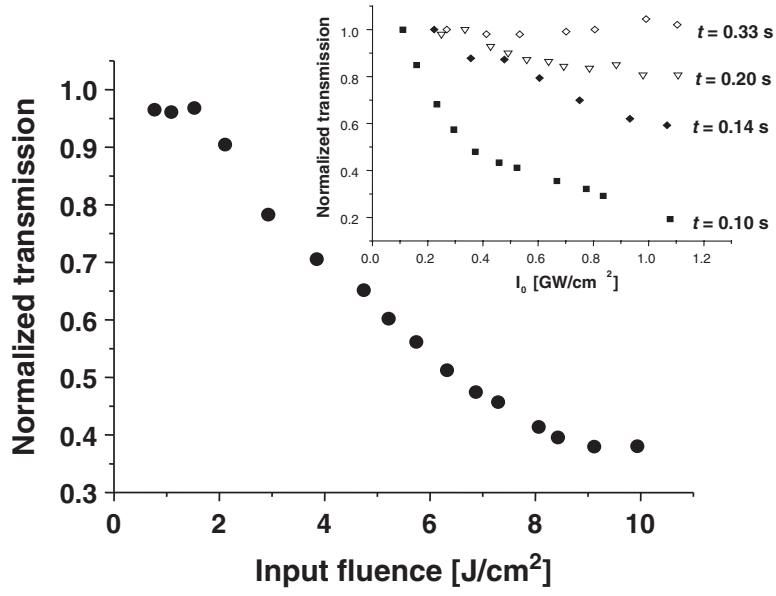

Figure 9. Non-linear transmission of silver–dendrimer nanocomposites $\{Ag(0)\}_E$ at 532 nm. Pulse repetition rate: 10 Hz. Inset: non-linear transmission results for $\{Ag(0)\}_E$ in a concentration of 2.95×10^{-4} mol/l at 532 nm, with the variation of the pulse repetition rate; t indicates the specific repetition periods. Reprinted with permission from [47], copyright (2000) of the American Chemical Society.

of the laser pulses was varied between 2 and 10 Hz. The result of the non-linear transmission measurement, with a pulse repetition rate of 10 Hz for a solution in a relatively low concentration of 2.0×10^{-4} mol/l is shown in figure 9 [47]. When the input fluence varies from 0.7 to 10.0 J/cm^2 (equivalent to the increase of the peak irradiance from 0.2 to 1.3 GW/cm^2) the transmission decreases by 62% [47]. The threshold fluence for optical limiting is around 2.0 J/cm^2. The optical-limiting performance of the silver–dendrimer nanocomposites compares well to the results obtained with novel organic structures such as: EHO–OPPE [163] (where a transmission drop of 65% was obtained between 0 and 0.6 GW/cm^2); the AF-380 dye [164] (exhibiting a threshold fluence of $\sim$2 J/cm^2 and a transmission loss of 60% for an input fluence increase up to 13 J/cm^2); and single-walled carbon nanotube suspensions [165] (showing a threshold fluence of $\sim$2 J/cm^2 and transmission decrease of 70% for fluence increasing up to 6 J/cm^2). Thus, it is now established that the Ag dendrimer nanocomposite system exhibits strong optical-limiting effects at 532 nm.

5.2. *The mechanism of non-linear transmission in dendrimer nanocomposites*

There have been investigations into the mechanism of the non-linear transmission properties in dendrimer nanocomposites [47, 59]. However, owing to the complexity of the metal particle morphology, there has not been a completely self-consistent mechanism that could explain the results obtained from all dendrimer nanocomposite architectures [59, 166]. There are certain important characteristics that may offer a plausible explanation for the mechanism. For example, the dependence of the solution concentration on the non-linear transmission behaviour has been investigated. The measurement of the optical-limiting effect with increasing concentration or ratio of the metal has been reported [47, 166]. As expected, the transmission's decrease was less effective with the reduction of the solution concentration [47]. Repeated measurement of several cycles by increasing and decreasing the peak irradiance between 0 and $\sim$1.3 GW/cm^2 was also reported. The optical-limiting processes occurring in the silver–dendrimer nanocomposites structure at 532 nm has also been investigated by using the open *z*-scan technique [47] in the same optical setup configuration, with 10 Hz pulse repetition rate. From the open *z*-scan results it can be concluded that drastic optical extinction, by a factor of 115, occurs for a concentrated solution (5.9×10^{-4} mol/l) of silver–dendrimer nanocomposites at the laser beam focus for a fluence of 3.3 J/cm^2 (relatively moderate input irradiance of 0.42 GW/cm^2) [47].

5.3. *The mechanism of non-linear transmission in other similar metal topologies*

There have been a number of reports which have probed the mechanism of non-linear transmission in other metal topologies as well. For example, the optical-limiting performance of gold nanoclusters protected by C_{60}–tpy have been investigated with 8 ns pulses at 532 nm by Zhu *et al.* [167]. The experimental results showed that the nanocomposite possesses an impressive optical-limiting effect in comparison to C_{60} in toluene [167]. The main mechanism of optical-limiting was attributed to the non-linear absorption and subsequently induced non-linear scattering during excitation of the pulse [167]. The optical-limiting performance of PVP-stabilized platinum nanoparticles in methanol has also been reported [101]. Here, a theoretical model based on Mie extinction theory was used to describe the strong non-linear optical-limiting behaviour of metal nanoparticles [101]. The theoretical analysis and experi-

mental results show that the principal mechanism for the optical-limiting effect in the platinum nanoparticles can be attributed to interband transition of platinum during the excitation of nanosecond pulses. These results offer the suggestion that strong non-linear absorption processes may arise in certain metal nanoparticle systems by either strong non-linear scattering mechanisms or interband excitations in the metal's electronic structure. Both of these processes are certainly possible in metal topologies contained in dendrimer nanocomposites.

5.4. *The time-dependence of the non-linear transmission effect*

Further understanding of the mechanisms of the optical-limiting effect in dendrimer nanocomposites may also require an understanding the time-scale of the effect [47, 57, 59]. In general, for optical excitation close to the linear absorption band, such as at 532 nm for the silver–dendrimer nanocomposites, the cross-sections for reverse saturable absorption (RSA) and non-linear scattering should be much higher than the cross-section for two-photon absorption [168]. Time-resolved photoluminescence measurements on silver–dendrimer nanocomposites have shown that the excited state lifetimes in metal–dendrimer nanocomposites are very short, of the order of picoseconds (see next section) [48]. RSA processes were seen to develop on a time-scale similar to the excited state lifetime. For example, Perry *et al.* [169] investigated phthalocyanine complexes bearing heavy atoms or paramagnetic groups, or in solvents containing heavy atoms, and showed these system exhibits enhanced optical limiting by excited triplet-state absorption. As in the case of certain nanocomposite systems, the excited state lifetime is usually in the nanosecond range [170]. It was thus suggested that the contribution of RSA is small for the silver–dendrimer nanocomposites since the lifetime of the excited state is extremely short [57]. Another approach when trying to explain the relatively slow optical-limiting effect observed in dendrimer nanocomposites is to consider processes that originate from absorption induced non-linear scattering [171]. As was mentioned before, for the case of Pt nanoparticles this effect can lead to impressive optical-limiting behaviour in metal particle topologies.

5.5. *Non-linear transmission in thin metal films*

There have been measurements on thin films containing metal nanoparticle architectures and these results seem to vary from the effects observed in the solution phase of dendrimer–metal nanocomposites. Smith *et al.* [172] used the *z*-scan technique at a similar wavelength (532 nm) to measure the non-linear absorption coefficient of approximately continuous 50 Å thick gold films, deposited on surface-modified quartz substrates. As was found with the dendrimer–metal nanocomposites, the highly absorbing metal films required analysis of both the real and imaginary parts of the susceptibility, using both open and closed *z*-scan measurements. Interestingly, when peak intensities of the order of $0.1\,GW/cm^2$ were used, a transmission decrease of ~8% was detected [172]. For intensities greater than $0.16\,GW/cm^2$ ablative damage occurred, which was observed by a sharp peak in the *z*-scan transmission which increased with each scan. This instability to intense laser pulses of the metal thin film material was also noted by an asymmetry in the baseline of the *z*-scan. While the magnitude of the effect may have been small in the metal thin film, the measured non-linear response could be described relatively well by mean field theories and a Fermi smearing mechanism [173]. The dendrimer nanocomposites appear to have much better stability to intense laser pulses and

larger non-linear optical responses as well. The dendrimer nanocomposites show smooth non-linear transmission and open *z*-scan curves. The silver–dendrimer nanocomposite too seems to be quite stable up to 1 GW/cm^2 [47]. This high stability was also seen in the ultra-fast time-resolved measurements [48].

5.6. *Non-linear transmission measurements in the infrared*

Non-linear transmission measurements of dendrimer nanocomposites have also been investigated at infrared wavelengths. For example, the non-linear transmission for both gold– and silver–dendrimer nanocomposites was reported with ns pulses at 1064 nm [166]. A significant effect was observed in both systems (although certainly not as strong as in the case of 532 nm excitation). For the gold nanocomposite system a decrease by 10% in the transmission was observed while for the silver nanocomposite a decrease of 12% was observed as the input fluence was varied from 1 to 15 J/cm^2 (which is proportional to an input irradiance range from 0.3 to 1.9 GW/cm^2) [166]. It is important to note that the pure dendrimer showed no significant non-linear transmission effect in comparison to the metal nanocomposites at the infrared excitation wavelength. This strongly suggests that the non-linear optical effects observed here for external structures originate mainly due in the contribution of the metal nanocomposites. In both cases (silver– and gold–dendrimer metal nanocomposites at 1064 nm) the data could be readily fitted to the model of two-photon absorption (TPA) [166]. The TPA coefficients thus obtained were 0.7 cm/GW for the silver and 0.5 cm/GW for the gold nanocomposites. According to previous theoretical work on the mechanisms responsible for large non-linear transmission (two-photon absorption) coefficients in organic polymers [174], the results at 1064 nm can be explained by possible resonantly enhanced TPA when the systems exhibit linear absorption peaks close to exactly half the TPA wavelength. Another possible mechanism of the non-linear absorption at 1064 nm is related to the geometry of the metal particle. For example in the case of metal nanorods, the process of infrared photochemical aggregation may be connected with the non-linear transmission results of the rods at 1064 nm [59]. In one report of non-linear transmission measurements of gold nanorods of aspect ratio 5.0, a small but measurable non-linear effect was observed, but no effect was reported for the sample with an aspect ratio of 3 [59]. This may be due to the fact that the surface plasmon absorption of the aspect ratio 3.0 rods is blue-shifted very much in comparison to the longer rod sample, and there was hardly any linear absorption at 1064 nm. It should be noted that the mechanism derived from the NLT results, which describes the effect observed from the rods, only involved aggregation of metal particles. However, this aggregation mechanism was not seen in the case of metal spheres or metal nanocomposites.

5.7. *Non-linear transmission in different metal–dendrimer topologies*

The non-linear transmission of different metal topologies have also been compared in a recent report [59]. The comparison of the non-linear effect of gold nanorods, spheres, and gold–dendrimer nanocomposites was investigated. The chromophore-functionalized dendrimer–metal nanocomposite, which contained an organic chromophore (dansyl) attached to the periphery of the dendrimer, was also investigated with and without the encapsulation of gold metal nanoparticles. This was done in order to compare the contribution of the gold metal particles to the non-linear transmission effect to that of the non-linear optical chromophore.

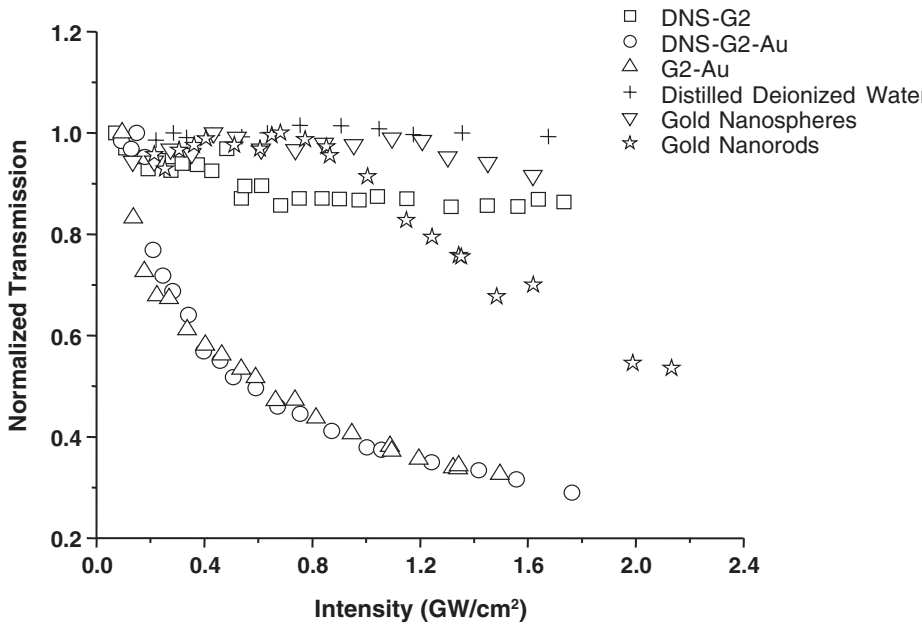

Figure 10. The comparison of NLT effects of gold rods, spheres, G2–NH_2–Au, DNS–G2, and DNS–G2–Au. In all the experiments the optical density at 532 nm was similar for the different metal topologies. Reprinted with permission from [59], copyright (2003) of the American Chemical Society.

The composite non-linear transmission result can be seen in figure 10. What was found from these measurements was that at 532 nm (and again with ns pulses), the functionalized dendrimer system (without metal nanoparticles) showed only a weak non-linear transmission effect (see figure 10). However, DNS–G2–Au showed a much stronger non-linear transmission effect [59]. The mechanism of this enhanced non-linear transmission effect may relate to the interaction of the metal particle with the attached chromophores. Steady-state fluorescence measurements were carried out for the investigation of these interactions. Fluorescence measurements showed the quenching processes to increase with increasing concentration of gold nanoparticles. It was suggested that the quenching results from the excited-state interactions via non-radiative energy transfer from the dye to the metal [126]. Thus, we would expect to observe a larger NLT effect for the chromophore-functionalized dendrimer–metal nanocomposite in comparison to the G2–NH_2–Au. However, the results of the two nanocomposites are comparable when metal concentrations are similar. This implies that the dominate NLT effect is due to the characteristics of the gold nanoparticles and that the NLT attributed to excited state absorption is relatively weak for the case of the chromophore-functionalized dendrimer system.

6. Pump–probe measurements of dendrimer nanocomposites

The excited-state dynamics of metal particles embedded in dendrimers has provided new information concerning the mechanism of electronic relaxation pathways in metal particles. As for other metal topologies, the field of ultra-fast dynamics has been paid much attention. The hot electron dynamics of gold particles as well as silver colloids in solution or in the solid state have been major issues in discerning

the mechanisms involved in the dynamics of the non-Fermi electron distribution relaxation back to an equilibrium distribution. A basic mechanism of the ultra-fast in-resonance (surface plasmon resonance) excitation involves the establishment of a non-Fermi distribution, which initially relaxes through electron–electron and electron–phonon relaxation steps giving rise to an excitation of the metal lattice (phonons). As the non-linear optical processes described above may involve the relaxation of excitation energy through energy transfer to the surrounding medium, this effect in metal particles in general is still an important and unanswered question.

6.1. *Pump–probe measurements in gold–dendrimer nanocomposites*

There has been one report of ultra-fast pump–probe measurements in dendrimer–metal nanocomposites. Kleiman *et al*. [148] have investigated gold dendrimer–metal nanostructures using ultra-fast two-colour pump–probe measurements at 800 nm. One representative dependence from this measurement is shown in figure 11. These measurements primarily probed the transient bleaching signals of the metal particles encapsulated in the PAMAM dendrimers. The transient bleaching signals corresponding to the gold–dendrimer nanocomposites showed primarily a single rapidly decaying component that recovers to equilibrium in less than 5 ps. It was also shown that the time constant for the transient bleaching signal increases with pump fluence [148]. This report confirmed suggestions that the dendrimer macromolecule can act as a stable passivating environment for the gold nanoparticles. This investigation

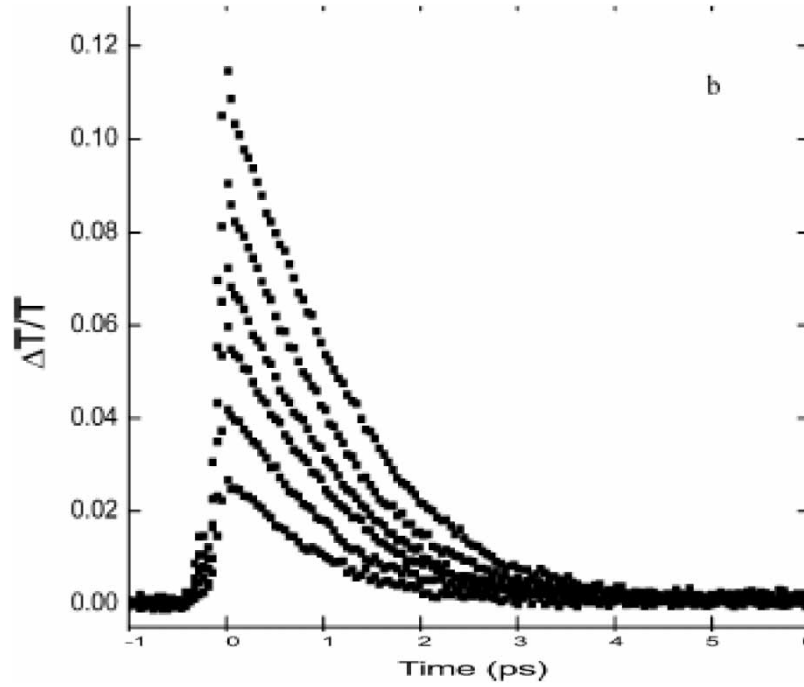

Figure 11. Gold–dendrimer metal nanocomposites investigated by transient absorption measurements for a G9 host of PAMAM [148]. The curves are for different excitation fluence, for example, 100, 200, 300, 400, 500, 600, and the biggest change in transmission was for 800 J/cm^2. Reprinted with permission from [148], copyright (2003) of the American Chemical Society.

suggested that the vibrational manifold of the dendrimer may act as a reservoir for the cooling processes electron–phonon and phonon–phonon interactions in the system.

6.2. *Electron–phonon coupling in metal particles*

It appears that the electron–phonon coupling process is indeed critical to understanding the excitation in metal nanoparticles. Although there have been no reports of ultra-fast emission investigations detailing this process, there have been reports of ultra-fast transient absorption measurements. Hartland *et al.* [175] have used femtosecond pump–probe methods to investigate the electron–phonon coupling process in metal particles. In this report, ultra-fast laser spectroscopy was used to characterize the low frequency acoustic breathing modes of Au particles, with diameters between 8 and 120 nm. It was shown that these modes are impulsively excited by the rapid heating of the particle lattice that occurs after laser excitation. This excitation mechanism is a two-step process: the pump laser deposits energy into the electron distribution, and this energy is subsequently transferred to the lattice via electron–phonon coupling. The measured frequencies of the acoustic modes are inversely proportional to the particle radius. Analysis of the data showed that an inhomogeneous decay dominates the damping, even for high quality samples (8–10% dispersion in the size distribution). The size dependence of the electron–phonon coupling constant was also examined for these particles. The results show that, within the signal noise of these measurements, the electron–phonon coupling constant does not vary with size for particles with diameters between 4 and 120 nm. Furthermore, the value obtained is the same as that measured for bulk gold [175].

7. Emission of nanoparticle topologies

The ultra-fast emission of metal nanocomposites has given new insight toward the understanding of enhanced emission in different metal particles of various geometrical shapes, as well as the mechanism of the emission in smaller metal particles. As stated above, the relatively low emission efficiency in metal nanoparticles suggests that continuous wave measurements without the aid of significant local field enhancement may not give much information concerning the emission properties of nanocomposites. There have been reports concerning the field enhancement as a result of the close proximity of the metal to organic molecules, where the emission of the organic molecule could be quantitatively monitored [176]. But, owing to the low efficiency in dendrimer nanocomposites, ultra-fast time-resolved emission measurements have been used to observe the very short-lived excited states and emission.

7.1. *Ultra-fast emission in gold– and silver–dendrimer nanocomposites*

The dynamics of emission for both silver and gold were reported first. A representative curve of the ultra-fast emission observed from the gold–dendrimer metal nanocomposite system is shown in figure 12. In this case the time-resolved emission from the gold nanocomposite sample was taken from excitation at 395 nm [48]. It is seen that the dynamics of the emission signal has at least two decay components. One of these decay components is comparable in duration with the width of the instrument response function (IRF) (also shown in figure 12 by the dashed line) while the second one is relatively long, on a time-scale of several picoseconds [48].

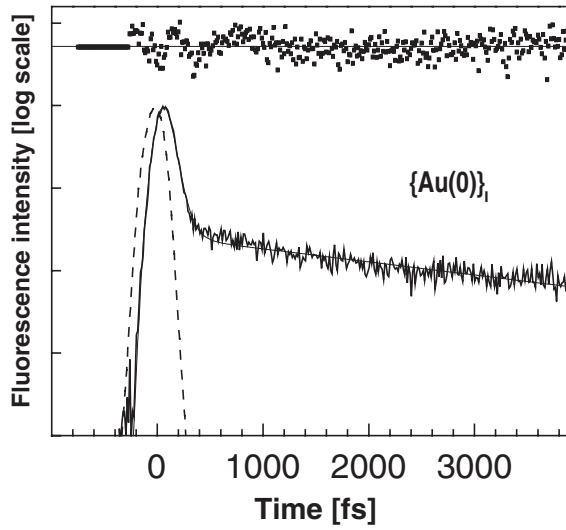

Figure 12. Fluorescence dynamics of $\{Au(0)\}_I$, for excitation at 395 nm, and emission at 570 nm. The corresponding numerical fits to the data are indicated by the thin solid lines. The residuals of the fit are shown at the top of the graph.

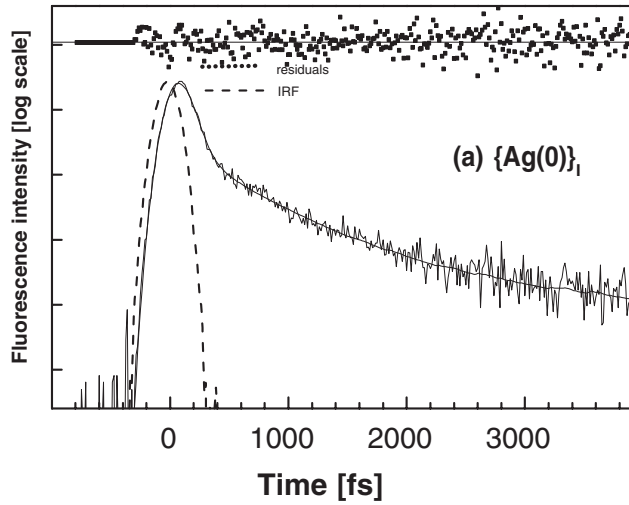

Figure 13. Fluorescence dynamics of $\{Ag(0)\}_I$, for excitation at 395 nm, and emission at 480 nm. The corresponding numerical fits to the data are indicated by the thin solid lines. Reprinted with permission from [48], copyright (2001) of the American Institute of Physics.

The emission dynamics of the nanocomposites was directly compared with the time-resolved emission from the host (PAMAM) dendrimer. The host dendrimer revealed a weak and slowly decaying fluorescence signal similar to the long decay component of the nanocomposite emission. This result, along with the polarization measurements that have also been carried out strongly suggests that the relatively long-lived fluorescence decay component may be connected with the host dendrimer, whereas the fast decaying component is associated with the metal emission [57].

It is interesting to note that the fast emission dynamics of silver–dendrimer metal nanocomposites are somewhat different from those obtained for gold nanocomposites when all other experimental parameters are held constant [48, 57]. For example, for optical excitation at 395 nm the gold–dendrimer nanocomposite ultra-fast emission could be reasonably well fitted by a two-exponential decay function with time constants of 74 fs, 5.5 ps and relative amplitudes 0.95, 0.05, respectively (best fit curve shown in figure 12) [48]. While the silver–dendrimer nanocomposite system did exhibit these two processes as well (an initial fast component followed by a slower decaying component, see figure 13), there was an additional intermediate decay component of approximately 650 fs. This additional component may be related to possible charge transfer processes that may occur from association of the silver nanoparticles with the PAMAM dendrimer host. The silver–dendrimer nanocomposites seemed to provide a stable environment for excitation by ultra-short pulses as well. This correlates well with the non-linear transmission measurements for the dendrimer–metal nanocomposites described above. The processes of excited state absorption or reverse saturable absorption may have some effect on the dynamics of emission in these systems as well.

7.2. *Ultra-fast emission in different metal topologies*

The ultra-fast dynamics in gold nanospheres and nanorods has been observed to be very similar to what was found with gold–dendrimer metal nanocomposites. The study of gold nanorods and nanospheres has also been carried out with ultra–fast upconversion setup [85]. A representative curve for the dynamics in this well-characterized metal topology is shown in figure 14. The observed emission (excited at

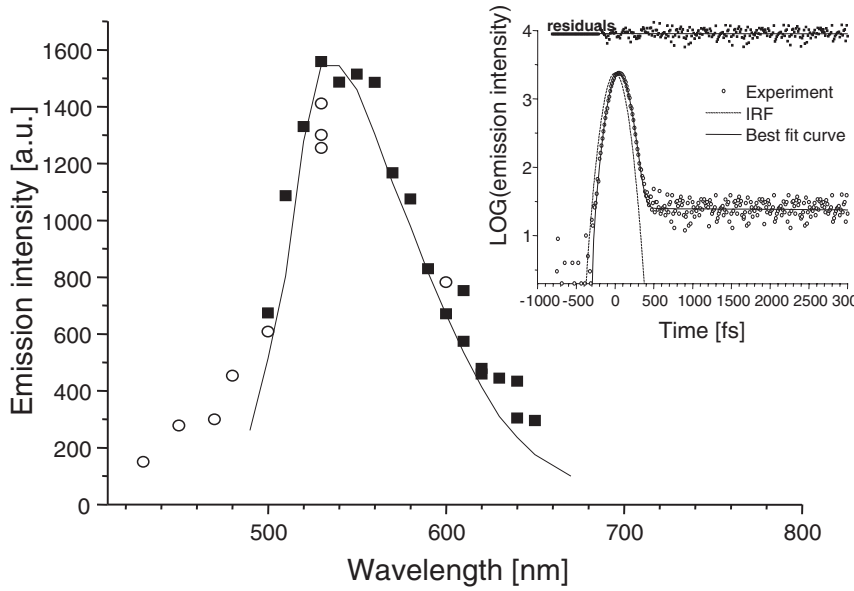

Figure 14. Spectrum of the fast component of gold nanospheres (SP). Solid squares: for excitation at 410 nm (3.02 eV), open circles: for excitation at 267 nm (4.65 eV). Insert: time-resolved emission from nanorods NR1. The best fit curve and instrument response function are also shown. Reprinted with permission from [85], copyright (2003) of the American Chemical Society.

400 nm) was found to be very fast. Estimation of the decay time by deconvolution procedures resulted in an emission decay time ≤ 50 fs. A very weak, long–lived component is also seen, which is similar to the case of gold–dendrimer metal nanocomposites. It was found in these experiments that the emission intensity was strictly and linearly dependent on the excitation power in the power range we used for excitation as expected. It was concluded that the measured fast emission dynamics was similar for both gold nanorods and nanospheres, and was not dependent on the emission wavelength. Further investigations with both gold nanorods and spheres also showed that when UV excitation pulses are used, the same fast dynamics of the observed emission was obtained. Ultra-fast anisotropy measurements were also carried out at both excitation regimes. It was found that the ultra-fast emission is depolarized with a residual anisotropy value close to zero, as was also the case with gold–dendrimer nanocomposites [85].

The fast emission spectrum of nanospheres obtained with 410 and 267 nm excitations has been reported in terms of understanding the mechanism of emission for gold nanoparticles [85]. It was observed that the fast emission peak emerges at about 530 nm independently of the excitation wavelength (see figure 14). This gives strong evidence that the observed emission is real luminescence originating from the relaxed state rather than scattering. The fact that the quantum efficiency of the emission excited at 267 nm was the same as that for excitation at 410 nm, as well as the depolarized character of the emission is inconsistent with the suggestion that the observed emission stems from the surface plasmon dipole emission after direct surface plasmon excitation by an incoming field. It was thus suggested that the ultra-fast emission originated from sp-electron–d-hole recombination, with the enhancement of the incoming and outgoing fields via plasmon resonances, as was proposed for the steady-state emission from copper and gold [95].

The ultra-fast emission spectra of gold nanorods also give information concerning the field enhancement effect observed in metal particles of different topologies. Reports have also shown the ultra-fast emission spectra of metal particles of different aspect ratios (as observed in figure 15). For example, for the two nanorod samples shown in figure 15, the spectra show broad peaks near the longitudinal SP resonance and a shoulder at about 530 nm. The calculated emission spectra for both nanorod samples have also been reported [85]. The initial recombination emission spectrum for bulk gold is taken either from Mooradian's experiment [141] or from a theoretical model developed by Apell *et al*. [177] (which are very close to each other). This spectrum has been multiplied by the enhancement factor calculated in accordance with the procedure described above. The result of these calculations fits relatively well to the experimental wavelength dependence of the ultra-fast emission. The strong correlation with the experimental data may give further evidence of an electron–d-hole recombination mechanism of the observed ultra-fast emission.

7.3. *Ultra-fast emission mechanism*

As mentioned above, various suggestions have contributed to the understanding of emission and transient absorption in gold nanoparticles. Part of the discussion has focused on the thermalization process of the non-Fermi distribution of electrons to a Fermi distribution, which may occur on a time-scale of hundreds of femtoseconds [20, 76, 78–80]. Interestingly, the ultra-fast emission observed here with both the gold nanorods and nanospheres occurs on a timescale of 50 fs (or faster), without detectable delay after excitation even for excitation far above Fermi level (267 nm,

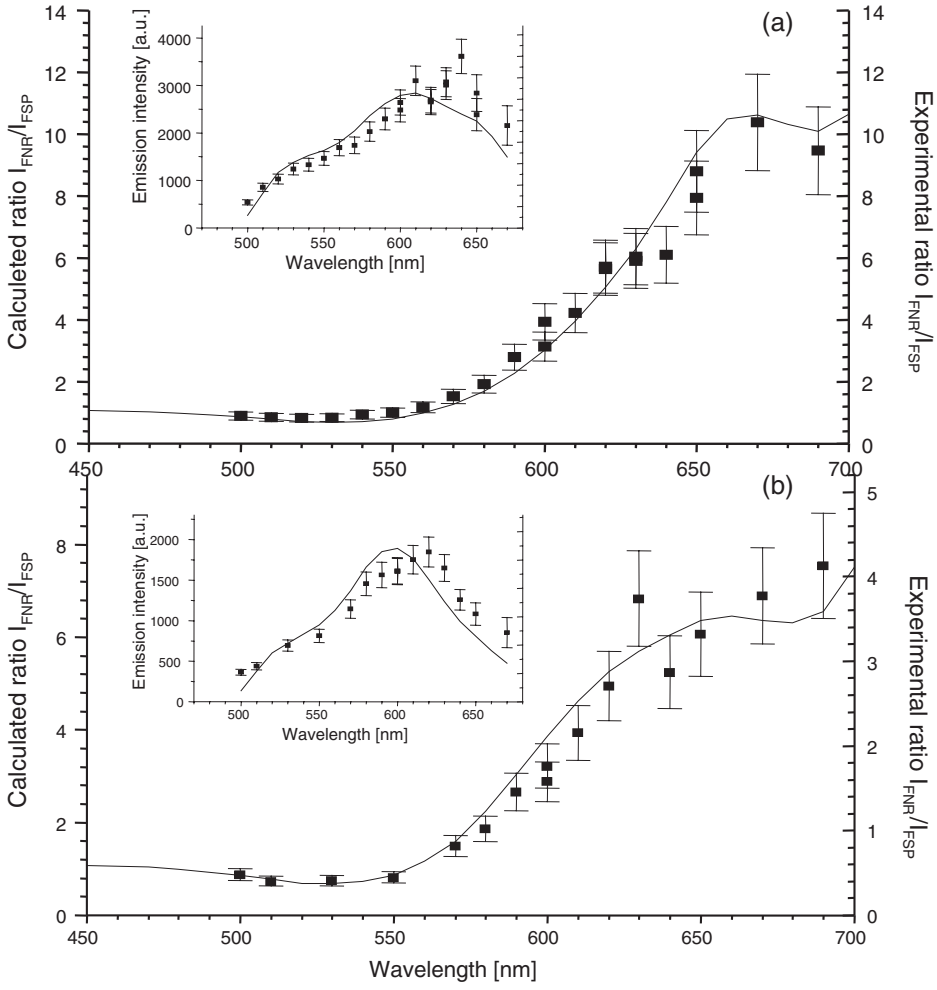

Figure 15. The ratio of the emission intensity from nanorods NR1 (a) and NR2 (b) to that of nanospheres. Spectra of the fast component of gold nanorods are shown in the respective insets. The result of numerical calculations for each case is also shown. Reprinted with permission from [85], copyright (2003) of the American Chemical Society.

$\hbar\omega_{exc} = 4.65\,\text{eV}$). This suggested that the formation and thermalization of 'hot' electrons in the excitation process may not be contributing processes to the emission we have investigated. Instead, the emission is strongly related to the dynamics of the d-holes created immediately after excitation. The interesting conclusion is that the hole relaxation within the d-band in momentum space to meet the momentum conservation for the radiative recombination for the electron near the Fermi level [95, 141] proceeds extremely fast, resulting in no detectable delay in the appearance of the emission in our experiment. It is also possible that the confinement in small particles lift the strict momentum conservation requirement and make the immediate recombination feasible. The lifetime of the recombination emission is limited by the lifetime of the d-holes. Although recent two-photon photoemission studies indicated that the holes in noble metals exhibit considerably longer lifetimes than electrons

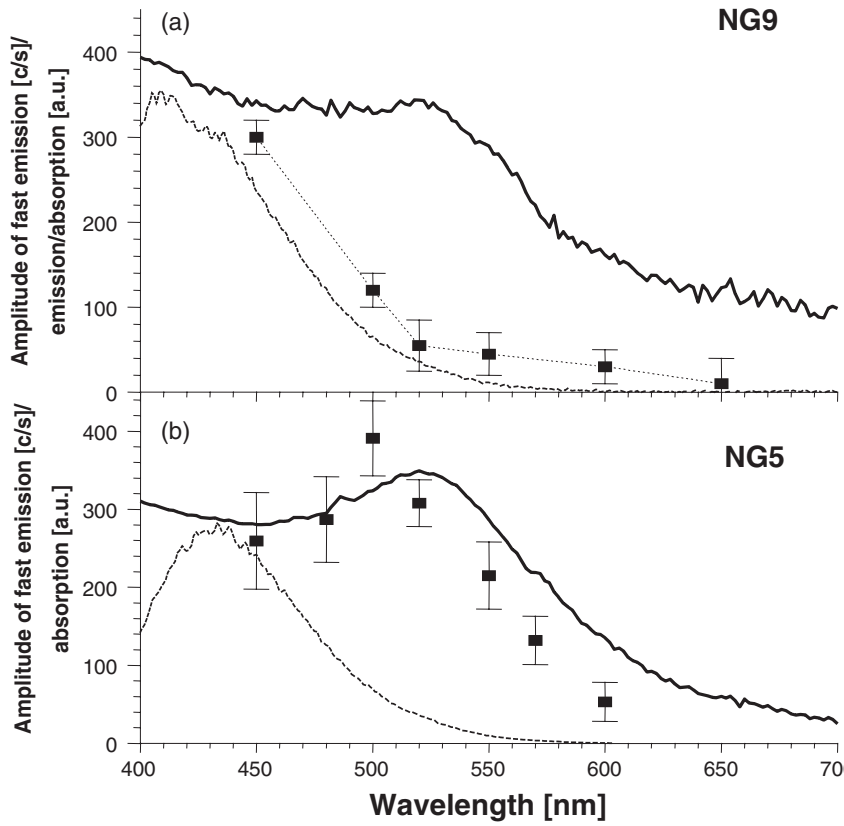

Figure 16. Comparison of the surface plasmon absorption resonance (solid line) with the wavelength dependence of the ultra-fast emission peak intensity (scatter graph) for excitation at 3.14 eV (395 nm). Intrinsic fluorescence spectra of pure G9 and G5 PAMAM dendrimers are also shown (dash lines).

of the same excitation energy, the electron–electron scattering into the empty states into the d-band holes remains on time-scales less than 100 fs [100, 178]. The fast nonradiative hole-filling process most likely happens through a process similar to the Auger process, as a result of energy conservation for electron–electron scattering, and it may lead to highly excited non-thermal electrons [78, 95, 177]. The lifetime of d-holes was estimated for copper to be about 20–30 fs [66, 100]. But the time-resolved emission measurements of the gold nanorods can give an upper limit of the lifetime of d-holes in gold nanoparticles of about 50 fs.

7.4. *Time-resolved emission in different dendrimer nanocomposite morphologies*

Time-resolved measurements have been used to describe the differences in metal topologies when different template methodologies are used. For example, when either PAMAM generations 5 or 9 (NG5 or NG9) were used, the dynamics of emission was found to be different. The relatively smaller nanoparticles were formed in the case of NG9 and relatively weak emission was observed. The wavelength dependence of the peak amplitude of the NG9 time-resolved emission was also reported (as seen in figure 16). The fluorescence spectrum of pure PAMAM dendrimer and absorption spectrum of NG9 were also given for comparison. It was observed that

there is a correlation of peak emission amplitude spectrum with the fluorescence spectrum of pure dendrimer rather than with surface plasmon resonance (SPR) of the nanocomposite NG9. This indicates that weak emission from NG9 is the intrinsic fluorescence from pure PAMAM G9. The fast and depolarized NG5 emission result, as well as the NG5 absorption spectrum is shown in figure 16(b). In this case the spectrum of the fast emission component correlates quite well with the SPR, but not with the emission spectrum of pure dendrimer (also shown in figure 16). This observation along with the depolarized character (see below) of the emission strongly suggests that the fast component in the NG5 emission is associated with the metal nanoparticle. The ultra-fast emission results for the dendrimer–metal nanocomposites correlate well with the model of intrinsic metal fluorescence strongly enhanced by the local field [21, 81, 157, 48, 85]. In both the NG5 and NG9 cases, the local environment of the metal particle is about the same, while the geometry is rather different for these nanocomposites. It is also important to note that the metal concentrations are about the same in both cases. Metal nanoparticles of complex, fractal-like shape with possible sharp edges in the case of NG5 might be one possible explanation that could bring about the much stronger local field enhancement, as compared to that of almost ideally spherical metal nanoparticles in the case of NG9 [71].

7.5. *Fluorescence anisotropy measurements in dendrimer nanocomposites*

The fluorescence anisotropy has also been used to provide information about the dipolar orientational dynamics occurring after the excitation of the nanocomposite systems. This technique has been successfully used to probe ultra-fast dynamics of energy transfer in organic conjugated dendrimers as well [151]. The anisotropy decay result for gold–dendrimer metal nanocomposites has been reported [48]. It was observed that the polarization state of the emission during the first 300 fs after excitation is quite different from that for longer times. The 'dip' and 'rise' in the anisotropy curve observed usually suggests that there are more than one species in the system whose contributions to the effective anisotropy have different time-scales [179]. Indeed, depolarized emission has been observed for metals [141], while initially highly polarized emission is typical for organics. From these observations we can attribute the polarized long decay to the emission of the dendrimer template and the fast (and nearly depolarized) component to the emission of the metal nanoparticle. This result is in agreement with the measurements of the pure dendrimer fluorescence decay described above. The nearly depolarized fast component in the emission dynamics suggests an incoherent character of the metal emission. This strongly supports the conclusion that the observed fast emission is indeed the fluorescence of the metal nanoparticle. The anisotropy in metal particles has also been investigated by other spectroscopic techniques. Pileni *et al.* [180] compared the optical properties of spherical particles organized in a two-dimensional (2D) structure with disordered and coalesced particles. Both particle preparations were deposited on cleaved graphite substrates. When particles are arranged in a hexagonal array, the optical measurements under p-polarization show a new high-energy resonance which is interpreted as a collective effect, resulting from optical anisotropy due to the mutual interactions between particles [180]. For disordered and coalesced particles, a low-energy resonance appears instead of the high-energy resonance observed for spherical and organized particles.

8. Future applications of dendrimer nanocomposites

The use of dendrimer–metal nanocomposites for novel optical applications has been demonstrated as the above discussion points out. However, for future device applications it is desired to move these composite materials into the solid state. Making solid-state thin films of these materials is not trivial, however, as most of the synthetic procedures involve aqueous solutions or dendrimer nanocomposite systems dissolved in methanol. However, there have been reports of procedures which have successfully made gold thin films of PAMAM dendrimer–metal nanocomposites. Balogh *et al.* [182] have used Langmuir–Blodgett techniques to produce thin solid films of gold–dendrimer nanocomposites which were ultimately transferred to hydrophilic silicon wafers. These systems were investigated by atomic force microscopy (AFM). From reflectivity measurements it was found that the thickness of the layers was smaller when transferred on silicon at the air–water interface because of bonding between the dendrimer nanocomposite groups and the substrate. Vossmeyer *et al.* [183] have used another methodology to prepare gold–dendrimer nanocomposite films which may subsequently be used for vapour-sensing applications. An assembly method of layer-by-layer fabrication was used involving alternating and repetitive exposure of amino-functionalized glass substrates to nanoparticle and dendrimer solutions. The resulting films appeared both porous and grainy. A striking feature observed here was the approximately linear increase in surface plasmon absorbance with the number of cycles. Also, compared to the solution measurements the absorption of the plasmon resonance in the film was red-shifted and it was suggested this was due to a change in the interaction of nanoparticles as well as a change in the dielectric environment [183]. This relatively high degree of surface roughness may be useful for future applications in the surface sensing of various chemical and biological agents as well as for surface-enhanced optical effects.

Dendrimer–metal nanocomposites have also been used in biological or medical applications. There appears to be growing interest in this direction owing to the immense opportunities offered to researchers for drug delivery and therapeutic procedures. For example, Balogh *et al.* [109] have used silver complexes of poly(amidoamine) (PAMAM) dendrimers as well as different {silver–PAMAM} dendrimer nanocomposite solutions for *in vitro* testing against *Staphylococcus aureus*, *Pseudomonas aeruginosa*, and *Escherichia coli* bacteria, using the standard agar overlay method. Both PAMAM silver salts and nanocomposites displayed considerable antimicrobial activity without any loss of solubility and activity, even in the presence of sulphate or chloride ions. It was also found that there was increased antimicrobial activity with dendrimer carboxylate salts. This was attributed to the very high local concentration (256 carboxylate groups around a 54 Å diameter sphere) of nanoscopic size silver composite particles that are accessible by microorganisms [109]. The silver domains are suggested to bind to the dendrimer with a calculated specific surface area of several thousand m^2/g. Mecking *et al.* [184] have also demonstrated the process of such antimicrobial behaviour of metal nanocomposites involving branched macromolecules. It was found from their investigation that hybrids of silver particles of 1 to 2 nm in size with highly branched amphiphilically modified polyethyleneimines adhere effectively to polar substrates providing environmentally friendly antimicrobial coatings [184]. Other dendrimer encapsulating particles have been used for biomedical applications such as probe moieties. In diagnostics, dendrimers that contain Gd(III) complexes have been used as

contrast agents in magnetic resonance imaging [185]. There is certainly more to be investigated about these novel materials; however, at this point the structural requirements of these processes and possible applications of dendrimer nanocomposites are evident. With further investigations in this area and new insight into the mechanisms and rational design, the area of biological and medical applications of dendrimer–metal nanocomposites may continue to be an emerging area of research and technology.

9. Conclusions

The intended message of this review was to illustrate the fact that the synthesis, measurements, and properties of the nanocomposite systems differ greatly from those of their bulk and surfactant-based nanoparticle counterparts. It is not accurate to say, however, that the properties of dendrimer–metal nanocomposites replace those of other small metal particle topologies or that the functionalized systems would replace the use of organic chromophores in certain optical applications. Instead, it is found that the optical properties of these systems allow for enhanced effects that had not been established previously. For example, the dendrimer–metal nanocomposites, which possess impressive optical-limiting properties of nanosecond green light laser pulses, were actually shown to have larger effects than their inorganic surfactant counterparts as well as particles of different aspect ratios. Perhaps the most significant way in which the optical-limiting properties of dendrimer nanocomposites differ from those of other nanoparticle topologies is through the analysis of the mechanism. Indeed, the mechanism and analysis of the enhancement of the optical-limiting behaviour in certain DNCs in comparison to other metal topologies are important issues that require the inclusion of parameters such as size, void space, pH, as well as functionalization of PAMAM. It appears that all of these parameters are very important in understanding the complexity of the optical effects in these materials. This ultimately leads back to the question of the electron dynamics in the excitation and relaxation of small metal particles. There had been a number of reports in this connection for other metal topologies; however, there was only one report of ultra-fast absorption in the literature. This investigation did demonstrate the possibility that the PAMAM could be acting as a void or host for the metal nanoparticles. While the absorption properties are important, in relation to understanding the mechanism of dynamics as well as enhancement of emission and sensing applications, there have been very extensive investigations of the ultra-fast emission in dendrimer–metal nanocomposites. Also, an important comparison has been carried out by us where we have characterized the ultra-fast emission decay and spectrum for different metal particles of different aspect ratios. After great analysis of the dynamics of emission from pure (micelle) metal topologies, it has been shown that the ultra-fast emission in dendrimer–metal nanocomposites behaves very similarly to the emission obtained from metal rods and spheres using surfactants. This is used as a comparison to the dynamics and magnitude of the enhanced emission observed in dendrimer–metal nanocomposites. The close analysis of the dynamics of emission of the dendrimer–metal nanocomposites, under different environmental conditions, gives important information regarding the future use of the dendrimer nanocomposite materials in biological (water-soluble) and technological applications in medicine. It is thus believed that the understanding obtained

from these detailed investigations will lead to further applications of dendrimer–metal nanocomposites.

Acknowledgements

T. G. III thanks the Army Research Office and the National Science Foundation for support of the research of his group presented in this review.

References

[1] L. Brus, Appl. Phys. A **53**, 465 (1991).
[2] C. B. Murray, C. R. Kagan, and M. G. Bawendi, Science **270**, 1335 (1995).
[3] J. T. Hu, T. W. Odom, and C. M. Lieber, Acc. Chem. Res. **32**, 435 (1999).
[4] C. J. Murphy, Science **298**, 2139 (2002).
[5] J. H. Burroughes, D. D. C. Bradley, A. R. Brown, R. N. Marks, K. Mackay, R. H. Friend, P. L. Burns, and A. Holmes, Nature **347**, 539 (1990).
[6] B. H. Cumpston, S. P. Ananthavel, S. Barlow, D. L. Dyer, J. E. Ehrlich, L. L. Erskine, A. A. Heikal, S. M. Kuebler, Y. S. Lee, D. McCord-Maughon, J. Q. Qin, H. Rockel, M. Rumi, X. L. Wu, S. R. Marder, and J. W. Perry, Nature **398**, 51 (1999).
[7] L. W. Tutt and A. Kost, Nature **356**, 225 (1992).
[8] E. Betzig, J. K. Trautman, T. D. Harris, J. S. Weiner, and R. L. Kostelak, Science **251**, 1468 (1991).
[9] W. Denk, J. H. Strickler, and W. W. Webb, Science **248**, 73 (1990).
[10] L. R. Dalton, A. W. Harper, R. Ghosn, W. H. Steir, M. Ziari, H. Fetterman, Y. Shi, R. V. Mustacich, A. K. Y. Jen, and K. J. Shea, Chem. Mater. **7**, 1060 (1995).
[11] A. M. Naylor, W. A. Goddard, G. Keifer, and D. A. Tomalia, J. Am. Chem. Soc. **111**, 2339 (1989).
[12] V. M. Agranovich, D. M. Basko, K. Schmidt, G. C. LaRocca, F. Bassani, S. Forrest, K. Leo, and D. Lidzey, Chem. Phys. **272**, 159 (2001).
[13] W. U. Huynh, J. J. Dittmer, and A. P. Alivisatos, Science **295**, 2425 (2002).
[14] J. Z. Zhang, Acc. Chem. Res. **30**, 423 (1997).
[15] C. D. Grant, A. M. Schwartzberg, T. J. Norman, and J. Z. Zhang, J. Am. Chem. Soc. **125**, 549 (2003).
[16] A. Henglein, Chem. Rev. **89**, 1861 (1989).
[17] J.-Y. Bigot, V. Halte, J.-C. Merle, and A. Daunois, Chem. Phys. **251**, 181 (2000).
[18] R. D. Averitt, S. L. Westcott, and N. J. Halas, J. Opt. Soc. Am. **16**, 1814 (1999).
[19] G. von Plessen, M. Perner, and J. Feldmann, Appl. Phys. B **71**, 381 (2000).
[20] C. Guillon, P. Langot, N. Del Fatti, and F. Vallee, New J. Phys. **5**, 13 (2003).
[21] S. Link and M. A. El-Sayed, Int. Rev. Phys. Chem. **19**, 409 (2000).
[22] N. Del Fatti, F. Vallee, C. Flytzanis, Y. Hamanaka, and A. Nakamura, Chem. Phys. **251**, 215 (2000).
[23] H. Inouye, K. Tanaka, I. Tanahashi, and K. Hirao, Phys. Rev. B **57**, 11334 (1998).
[24] D. L. Jeanmaire and R. P. van Duyne, J. Electroanal. Chem. **84**, 1 (1977).
[25] J. Kinugasa, S. Shimada, H. Matsuda, H. Nakanishi, and T. Kobayashi, Chem. Phys. Lett. **287**, 639 (1998).
[26] A. Wokaum, H. D. Lutz, A. P. King, U. P., Wild, and R. R. Ernst, J. Chem. Phys. **79**, 509 (1983).
[27] R. Breinbauer and E. N. Jacobsen, Angew. Chem., Int. Ed. **39**, 3604 (2000).
[28] M. Faraday, Phil. Trans. R. Soc. **147**, 145 (1857).
[29] M. Li, H. Schnablegger, and S. Mann, Nature **402**, 393 (1999).
[30] V. T. Liveri, Curr. Top. Colloid Interface Sci. **3**, 65 (1999).
[31] Dong-S. Bae, Kyong-S. Han, and J. H. Adair, J. Am. Chem. Soc. **85**, 1321 (2002).
[32] M. Antonietti, F. Gröhn, J. Hartmann, and L. Bronstein, Angew. Chem., Int. Ed. Engl. **36**, 2080 (1997).
[33] R. W. J. Scott, A. K. Datye, and R. M. Crooks, J. Am. Chem. Soc. **125**, 3708 (2003).
[34] L. Balogh and D. A. Tomalia, J. Am. Chem. Soc. **120**, 7355 (1998).
[35] K. Esumi, A. Suzuki, N. Aihara, K. Usui, and K. Torigoe, Langmuir **14**, 3157 (1998).

[36] H. C. Choi, W. Kim, D. Wang, and H. Dai, J. Phys. Chem. B **106**, 12361 (2002).
[37] K. Esumi and K. Torigoe, Prog. Colloid Polym. Sci. **117**, 80 (2001).
[38] A. Manna, T. Imae, K. Aoi, M. Okada, and T. Yogo, Chem. Mater. **13**, 1674 (2001).
[39] Y. Li and M. A. El-Sayed, J. Phys. Chem. B **105**, 8938 (2001).
[40] F. Gröhn, G. Kim, B. J. Bauer, and E. J. Amis, Macromolecules **34**, 2179 (2001).
[41] R. M. Crooks, B. I. Lemon III, L. Sun, L. K. Yeung, and M. Zhao, Top. Curr. Chem. **212**, 81 (2001).
[42] Y. Niu, L. K. Yeung, and R. M. Crooks, J. Am. Chem. Soc. **123**, 6840 (2001).
[43] M. Zhao and R. M. Crooks, Adv. Mater. **11**, 217 (1999).
[44] L. P. Balogh, S. S. Nigavekar, A. C. Cook, L. Minc, and M. K. Khan, PharmaChem **2**, 94 (2003).
[45] F. Gröhn, X. Gu, H. Gruell, J. C. Meredith, G. Nisato, B. J. Bauer, A. Karim, and E. J. Amis, Macromolecules **35**, 4852 (2002).
[46] J. Alvarez, L. Sun, and R. M. Crooks, Chem. Mater. **14**, 3995 (2002).
[47] R. G. Ispasoiu, L. Balogh, O. P. Varnavski, D. A. Tomalia, and T. Goodson, J. Am. Chem. Soc. **122**, 11005 (2000).
[48] O. Varnavski, R. G. Ispasoiu, L. Balogh, D. A. Tomalia, and T. Goodson III, J. Chem. Phys. **114**, 1962 (2001).
[49] V. Vicinelli, P. Ceroni, M Maestri, V. Balzani, M. Gorka, and F. Voegtle, J. Am. Chem. Soc. **124**, 6461 (2002).
[50] V. Balzani, P. Ceroni, A. Juris, M. Venturi, S. Campagna, F. Puntoriero, and S. Serroni, Coord. Chem. Rev. **219–221**, 545 (2001).
[51] K. Kuiki, Y. Koike, and Y. Okamoto, Chem. Rev. **102**, 2347 (2002).
[52] J. Kido and Y. Okamoto, Chem. Rev. **102**, 2357 (2002).
[53] D. Parker, Coord. Chem. Rev. **205**, 109 (2000).
[54] B. Savoini, J. E. Muñoz Santiuste, and R. González, Phys. Rev. B **56**, 5856 (1997).
[55] T.-S. Kang, B. S. Harrison, T. J. Foley, A. S. Knefely, J. M. Boncella, J. R. Reynolds, and K. S. Schanze, Adv. Mater. **15**, 1093 (2003).
[56] G. A. Hebbink, J. W. Stouwdam, D. N. Reinhoudt, and F. C. J. M. Van Veggel, Adv. Mater. **14**, 1147 (2002).
[57] T. Goodson III, in *Dendrimers and Other Dendritic Polymers*, edited by J. M. J. Frechet and D. A. Tomalia (John Wiley & Sons Ltd.), p. 515 (2001).
[58] J. S. Shirk, *Optical Limiting Properties of Phthalocyanines in Phthalocyanines: Properties and Applications*, Vol. 4, edited by C. C. Leznoff and A. B. P. Lever (VCH Publishers) (1995).
[59] R. West, Y. Wang, and T. Goodson III, J. Phys. Chem. B **107**, 3419 (2003).
[60] S. M. Milas, J. Y. Ye, T. B. Norris, L. P. Balogh, J. R. Baker, jr., K. W. Hollman, S. Emelianov, and M. O'Donnel, Appl. Phys. Lett. **82**, 994 (2003).
[61] W. E. Lawrence and J. W. Wilkins, Phys. Rev. B **7**, 2317 (1973).
[62] B. R. Cooper, H. Ehrenreich, and H. R. Philipp, Phys. Rev. **138**, A494 (1965).
[63] U. Kreibig and M. Vollmer, *Optical Properties of Metal Clusters* (Berlin: Springer) (1995).
[64] M. M. Alvarez, J. T. Khoury, T. G. Schaaff, M. N. Shafigullin, I. Vezmar, and R. L. Whetten, J. Phys. Chem. B **101**, 3706 (1997).
[65] S. Link, M. A. El-Sayed, T. G. Schaaf, and R. L. Whetten, Chem. Phys. Lett. **356**, 240 (2002).
[66] U. Kreibig, G. Bour, A. Hilger, and M. Gartz, Phys. Stat. Sol. **175**, 351 (1999).
[67] A. J. Haes and R. P. Van Duyne, J. Am. Chem. Soc. **124**, 10596 (2002).
[68] H. A. Clark, R. Kopelman, R. Tjalkens, and M. A. Philbert, Anal. Chem. **71**, 4837 (1999).
[69] M. Brasuel, R. Kopelman, J. W. Aylott, H. Clark, H. Xu, M. Hoyer, T. J. Miller, R. Tjalkens, and M. A. Philbert, Sensor Mater. **14**, 309 (2002).
[70] A. Bielinska, J. D. Eichman, I. Lee, J. R. Baker, and L. Balogh, J. Nanopart. Res. **4**, 395 (2002).
[71] O. Varnavski, F. Gröhn, B. J. Bauer, E. J. Amis, and T. Goodson III, Synth. Met. (submitted) (2003).
[72] J. H. Hodak, I. Martini, and G. V. Hartland, J. Phys. Chem. B **102**, 6958 (1998).
[73] S. Link and M. A. El-Sayed, J. Chem. Phys. B **103**, 8410 (1999).

[74] C. Voisin, N. Del Fatti, D. Christofilos, and F. Vallee, J. Phys. Chem. B **105**, 2264 (2001).
[75] J.-Y. Bigot, J.-C. Merle, O. Cregut, and A. Daunois, Phys. Rev. Lett. **75**, 4702 (1995).
[76] C.-K. Sun, F. Vallee, L. H. Acioli, E. P. Ippen, and J. G. Fujimoto, Phys. Rev. B **50**, 15337 (1994).
[77] C. Voisin, D. Christofilos, N. Del Fatti, F. Vallee, B. Pevel, E. Cottancin, J. Lerme, M. Pellarin, and M. Broyer, Phys. Rev. Lett. **85**, 2200 (2000).
[78] S. Link, S. Burda, Z. L. Wang, and M. A. El-Sayed, J. Chem. Phys. **111**, 1255 (1999).
[79] J. Cao, Y. Gao, H. E. ElSayed-Ali, R. J. D. Miller, and D. A. Mantell, Phys. Rev. B **58**, 10948 (1998).
[80] H. Petek, H. Nagano, M. J. Weida, and S. Ogawa, Chem. Phys. **251**, 71 (2000).
[81] M. B. Mohamed, V. Volkov, S. Link, and M. A. El-Sayed, Chem. Phys. Lett. **317**, 517 (2000).
[82] C. Sönnichsen, T. Franzl, T. Wilk, G. von Plessen, and G. Feldmann, Phys. Rev. Lett. **88**, 077402 (2002).
[83] B. Nikoobakht, J. Wang, and M. A. El-Sayed, Chem. Phys. Lett. **366**, 17 (2002).
[84] C. V. Hartland, M. Hu, O. Wilson, P. Mulvaney, and J. E. Sader, J. Phys. Chem. B **106**, 743 (2002).
[85] O. P. Varnavski, M. B. Mohamed, M. A. El-Sayed, and T. Goodson III, J. Phys. Chem. B **107**, 3101 (2003).
[86] M. Fleischman, P. J. Hendra, and A. J. McQuillan, Chem. Phys. Lett. **26**, 163 (1974).
[87] M. G. Albrecht and J. A. Creighton, J. Am. Chem. Soc. **99**, 5215 (1977).
[88] M. Moskovits, Rev. Mod. Phys. **57**, 783 (1985).
[89] A. Campion and P. Kambhampati, Chem. Soc. Rev. **27**, 241 (1998).
[90] J. Gersten and A. Nitzan, J. Chem. Phys. **73**, 3023 (1980).
[91] G. T. Boyd, Th. Rasing, J. R. R. Leite, and Y. R. Shen, Phys. Rev. B **30**, 519 (1984).
[92] J. Gersten and A. Nitzan, 1981, J. Chem. Phys. **75**, 1139 (1981).
[93] D. S. Wang and M. Kerker, Phys. Rev. B **24**, 1777 (1981).
[94] C. K. Chen, T. F. Heinz, D. Ricard, and Y. R. Shen, Phys. Rev. B **27**, 1965 (1983).
[95] G. T. Boyd, Z. H. Yu, and Y. R. Shen, Phys. Rev. B **33**, 7923 (1986).
[96] J. Kümmerlen, A. Leitner, H. Brunner, F. R. Aussenegg, and A. Wokaun, Mol. Phys. **80**, 1031 (1993).
[97] G. M. Goncher, and C. B. Harris, J. Chem. Phys. **77**, 3767 (1982).
[98] E. J. Hailwail and R. M. Hochstrasser, J. Chem. Phys. **82**, 4762 (1985).
[99] A. Wokaum, J. P. Gordon, and P. F. Liao, Phys. Rev. Lett. **48**, 957 (1982).
[100] M. Perner, P. Bost, U. Lemmer, G. von Plessen, and J. Feldmann, Phys. Rev. Lett. **78**, 2192 (1997).
[101] S. Qui, Y. Song, H. Liu, Y. Wang, Y. Gao, S. Liu, X. Zhang, Y. Li, and D. Zhu, Opt. Commun. **203**, 283 (2002).
[102] F. Gröhn, B. J. Bauer, Y. A. Akpalu, C. L. Jackson, and E. J. Amis, Macromolecules **33**, 6042 (2000).
[103] J. Zheng, J. T. Petty, and R. M. Dickson, J. Am. Chem. Soc. **125**, 7780 (2003).
[104] M. Zhao and R. M. Crooks, Chem. Mater. **11**, 3379 (1999).
[105] M. Zhao, L. Sun, and R. M. Crooks, J. Am. Chem. Soc. **120**, 4877 (1998).
[106] J. R. Lackowicz, I. Gryczynski, G. Piszczek, and C. J. Murphy, J. Phys. Chem. B **106**, 5365 (2002).
[107] V. Germain, J. Li, D. Ingert, Z. L. Wang, and M. P. Pileni, J. Phys. Chem. B **107**, 8717 (2003).
[108] The Aldrich company sells 34 kinds of PAMAM dendrimers.
[109] Y.-S. Seo, K.-S. Kim, K. Shin, H. White, M. Rafailovich, J. Sokolov, B. Lin, H. J. Kim, C. Zhang, and L. Balogh, Langmuir **18**, 5927 (2002).
[110] F. Seker and A. B. Ellis, Macromolecules **33**, 582 (2000).
[111] J. C. Garcia-Martinez, R. W. J. Scott, and R. M. Crooks, J. Am. Chem. Soc. **125**, 11190 (2003).
[112] M. Zhao, L. Sun, and R. M. Crooks, Polymer Preprints **40**, 400 (1999).
[113] L. Balogh, R. Valluzzi, K. S. Laverdure, S. P. Gido, G. L. Hagnauer, and D. A. Tomalia, J. Nanoparticle. Res. **1**, 353 (1999).
[114] W. Chen, D. A. Tomalia, and J. L. Thomas, Macromolecules **33**, 9169 (2000).

[115] C. L. Larson and S. A. Tucker, Appl. Spectrosc. **55**, 679 (2001).
[116] D. L. Richter-Egger, J. C. Landry, A. Tesfai, and S. A. Tucker, J. Phys. Chem. A **105**, 6826 (2001).
[117] K. R. Gopidas, J. K. Whitesell, and M. A. Fox, J. Am. Chem. Soc. **125**, 6491 (2003).
[118] A. Taubert, U. M. Wiesler, and K. Müllen, J. Mater. Chem. **13**, 1090 (2003).
[119] S. Nakao, K. Torigoe, K. Kon-No, and T. Yonezawa, J. Phys. Chem. B **106**, 12097 (2002).
[120] C. M. Cardona, T. Wilkes, W. Ong, A. E. Kaifer, T. D. McCarley, S. Pandey, G. A. Baker, M. N. Kane, S. N. Baker, and F. V. Bright, J. Phys. Chem. B **106**, 8649 (2002).
[121] A. E. Kaifer, C. M. Cardona, J. Alvarez, and Y. Wang, Polym. Mater. Sci. Eng. **84**, 853 (2001).
[122] U. Hahn, M. Gorka, F. Vogtle, V. Vicinelli, P. Ceroni, M. Maestri, and V. Balzani, Angew. Chem., Int. Ed. **41**, 3595 (2002).
[123] S. Huang, L. Fu, X. Zhang, H. Liu, W. Li, and R. Zhuo, Sci. China, Ser. B **46**, 271 (2003).
[124] B. Yoza, A. Arakaki, K. Maruyama, H. Takeyama, and T. Matsunaga, J. Biosci. Bioeng. **95**, 21 (2003).
[125] R. R. Chance, A. Prock, and R. Silbey, Adv. Chem. Phys. **37**, 1 (1978).
[126] E. Dulkeith, A. C. Morteani, T. Niedereichholz, T. A. Klar, J. Feldmann, S. A. Levi, F. C. J. M. van Veggel, D. N. Reinhoudt, M. Möller, and D. I. Gittins, Phys. Rev. Lett. **89**, 203002 (2002).
[127] Y. Wang and T. Goodson III, Macromolecules (submitted) (2003).
[128] L. H. Slooff, A. van Blaaderen, A. Polman, G. A. Hebbink, S. I. Klink, F. C. J. M. van Veggel, D. N. Reinhoudt, and J. W. Hofstraat, J. Appl. Phys., **91**, 3955 (2002).
[129] H. Gerald, PhD thesis, available in print: http://www.tup.utwente.nl/catalogue/book/index.jsp?isbn=9036517869 (2002).
[130] S. H. Benjamin, PhD thesis, University of Florida (2003).
[131] Y. Wang and T. Goodson III, Chem. Commun. (submitted) (2003).
[132] M. Kawa and J. M. J. Fréchet, Chem. Mater. **10**, 286 (1998).
[133] L. Zhu, X. Tong, M. Li, and E. Wang, J. Phys. Chem. B **105**, 2461 (2001).
[134] M. Takahashi, Y. Hara, K. Aoshima, H. Kurihara, T. Oshikawa, and M. Yamashita, Tetrahedron Lett. **41**, 8485 (2000).
[135] M. Pietraszkiewicz, J. Karpiuk, and K. Staniszewski, J. Alloys Compd. **341**, 267 (2002).
[136] P. Ceroni, V. Viccinelli, M. Maestri, V. Balzani, S. Gestermann, C. Kauffmann, M. Gorka, and F. Voegtle, Polym. Mater. Sci. Eng. **84**, 230 (2001).
[137] F. Voegtle, G. Marius, V. Vicinlli, P. Ceroni, M. Maestri, and V. Balzani, Chemphyschem **12**, 769 (2001).
[138] A. P. Alivisatos, J. Phys. Chem. **100**, 13226 (1996).
[139] C. Bohren and D. R. Huffman, *Absorption and Scattering of Light by Small Particles* (John Wiley and Sons) (1983).
[140] C. L. Haynes, A. D. McFarland, L. L. Zhao, R. P. Van Duyne, and G. C. Schatz, J. Phys. Chem. **107**, 7337 (2003).
[141] A. Mooradian, Phys. Rev. Lett. **22**, 185 (1969).
[142] Y.-M. Hwang, D. H. Jeong, H. J. Shih, D. Kim, S. C. Jeong, S. H. Han, J.-S. Lee, and G. Cho, J. Phys. Chem. B **106**, 7581 (2002).
[143] M. Hu and C. V. Hartland, J. Phys. Chem. B **106**, 7029 (2002).
[144] S. Link, C. Burda, M. B. Mohamed, B. Nikoobakht, and M. A. El-Sayed, Phys. Rev. B **61**, 6086 (2000).
[145] V. Halte, J.-Y. Bigot, B. Palpant, M. Broyer, B. Prevel, and A. Perez, Appl. Phys. Lett. **75**, 3799 (1999).
[146] M. Perner, S. Gresillon, J. März, G. von Plessen, and J. Feldmann, Phys. Rev. Lett. **85**, 792 (2000).
[147] A. Arboet, C. Voisin, D. Christofilos, Del Fatti, N. Langot, F. Vallee, J. Lerme, J. Celep, E. Cottancin, M. Gaudry, M. Pellarin, M. Broyer, M. Maillard, M. P. Pileni, and M. Trguer, Phys. Rev. Lett. **90**, 177401 (2003).
[148] J. S. Melinger, V. A. Kleiman, D. McMorrow, F. Gröhn, B. J. Bauer, and E. J. Amis, Phys. Chem. A **107**, 3424 (2003).

[149] O. Varnavski, S. A. Lahankar, L. Sukhomlinova, R. Twieg, and T. Goodson III, J. Phys. Chem. B **120**(1) (in press) (2004).
[150] O. Varnavski, A. Leanov, L. Liu, J. Takacs, and T. Goodson III, Phys. Rev. B **15**, 114 (2000).
[151] M. I. Ranasinghe, O. P. Varnavski, J. Pawlas, S. I. Hauck, J. Louie, J. F. Hartwig, and T. Goodson III, J. Am. Chem. Soc. **124**, 6520 (2002).
[152] M. I. Ranasinghe, Y. Wang, and T. Goodson III, J. Am. Chem. Soc. **125**, 5258 (2003).
[153] A. Henglien, J. Phys. Chem. **97**, 5457 (1993).
[154] G. Mie, Ann. Phys. (Leipzig) **25**, 377 (1908).
[155] C. Sönnichsen, T. Franzl, T. Wilk, G. von Plessen, and G. Feldmann, New J. Phys. **4**, 93 (2002).
[156] J. A., He, R. Valluzzi, K. Yang, T. Dolukhanyan, C. Sung, J. Kumar, and S. K. Tripathy, Chem. Mater. **11**, 3268 (1999).
[157] T. J. Prosa, B. J. Bauer, E. J. Amis, D. A. Tomalia, and R. J. Scherrenberg, Polym. Sci. **35**, 2913 (1997).
[158] S. Klingelhöfer, W. Heitz, A. Greiner, S. Oestreich, S. Förster, and M. Antonietti., J. Am. Chem. Soc. **119**, 10116 (1997).
[159] N. Sun, Y. Wang, Y. Song, Z. Guo, L. Dai, and D. Zhu, Chem. Phys. Lett. **334**, 277 (2001).
[160] L. Francois, M. Mostafavi, J. Belloni, and J. A. Delaire, Phys. Chem. Chem. Phys. **3**, 4965 (2001).
[161] Y. P. Sun, J. E. Riggs, K. B. Henbest, and R. B. Martin, J. Nonlinear Opt. Phys. Mater. **9**, 481 (2000).
[162] K. S. Bindra, S. M. Oak, and K. C. Rustagi, Opt. Commun. **124**, 452 (1996).
[163] G. S. He, C. Weder, P. Smith, and P. Prasad, IEEE J. Quantum Electron. **34**, 2279 (1998).
[164] M. P. Joshi, J. Swiatkiewicz, F. Xu, P. Prasad, B. A. Reinhardt, and R. Kannan, Opt. Lett. **23**, 1742 (1998).
[165] S. R. Mishra, H. S. Rawat, S. C. Mehendale, K. C. Rustagi, A. K. Sood, R. Bandyopadhyay, A. Govindaraj, and C. N. R. Rao, Chem. Phys. Lett. **317**, 510 (2000).
[166] Y. Jin, L. P. Balogh, D. A. Tomalia, and T. Goodson III, unpublished results.
[167] S. L. Qu, S. Y. Fu, H. J. Li, Y. H. Geng, Y. L. Song, S. T. Liu, Y. L. Li, and D. Zhu, Chin. Phys. Lett. **19**, 1811 (2001).
[168] S. S. Harilal, C. V. Bindhu, V. P. N. Nampoori, and C. P. G. Vallabhan, J. Appl. Phys. **86**, 1388 (1999).
[169] J. W. Perry, K. Mansour, I.-Y.S. Lee, X.-L. Wu, P. V. Bedworth, C. T. Chen, D. Ng, S. R. Marder, P. Miles, T. Wada, M. Tian, and H. Sasabe, Science **273**, 1533 (1996).
[170] J. W. Perry, 'Organic and metal-containing reverse saturable absorbers for optical limiting', in *Nonlinear Optics of Organic Molecules and Polymers*, edited by H. S. Nalwa and S. Miyata (Boca Raton: CRC Press) (1997).
[171] O. Durand, V. Grolier-Mazza, and R. Frey, J. Opt. Soc. Am. **16**, 1431 (1999).
[172] D. D. Smith, Y. Yoon, R. W. Boyd, J. K. Campbell, L. A. Baker, R. M. Crooks, and M. George, J. Appl. Phys. **86**, 6200 (1999).
[173] F. Hache, O. Ricard, C. Flytzanis, and U. Kreibig, Appl. Phys. A: Solids Surf. **47**, 347 (1998).
[174] T. Kogej, D. Beljonne, F. Meyers, J. W. Perry, S. R. Marder, and J. L. Bredas, Chem. Phys. Lett. **298**, 1 (1998).
[175] J. H. Hodak, A. Henglein, and G. V. Hartland, J. Chem. Phys. **111**, 8613 (1999).
[176] K. Sokolov, G. Chumanov, and T. M. Cotton, Anal. Chem. **70**, 3898 (1998).
[177] P. Apell, R. Monreal, and S. Lundquist, Phys. Scr. **38**, 174 (1988).
[178] R. Matzdorf, A. Gerlach, F. Theilmann, G. Meister, and A. Goldmann, Appl. Phys. B **68**, 393 (1999).
[179] J. R. Lakowicz, *Principles of Fluorescence Spectroscopy* (New York: Kluwer), chapter 11 (1999).
[180] A. Taleb, V. Russier, A. Courty, and M. P. Pileni, Appl. Surf, Sci. **162/163**, 655 (2000).

[181] K. Shibamoto, K. Katayama, M. Fujinami, and S. Tsuguo, Anal.Sci. **17**, S255 (special issue) (2001).
[182] L. Balogh, D. R. Swanson, D. A. Tomalia, G. L. Hagnauer, and A. T. McManus, NanoLetters **1**, 18 (2001).
[183] N. Krasteva, I. Besnard, B. Guse, R. E. Bauer, K. Müllen, A. Vasuda, and T. Vossmeyer, NanoLetters **5**, 551 (2002).
[184] C. Aymonier, U. Schlotterbeck, L. Antonietti, P. Zacharias, R. Thomann, J. C. Tiller, and S. Mecking, Chem. Commun. **24**, 3018 (2002).
[185] S. E. Stiriba, H. Frey, and R. Haag, Angew. Chem., Int. Ed. **41**, 1329 (2000).